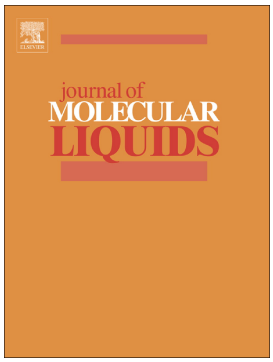

Theorical investigation of adsorption mechanism of doxorubicin anticancer drug on the pristine and functionalized single-walled carbon nanotube surface as a drug delivery vehicle: A DFT study

Sina Karimzadeh, Babak Safaei, Tien-Chien Jen

PII: S0167-7322(20)37132-4

DOI: https://doi.org/10.1016/j.molliq.2020.114890

Reference: MOLLIQ 114890

To appear in: *Journal of Molecular Liquids*

Please cite this article as: S. Karimzadeh, B. Safaei and T.-C. Jen, Theorical investigation of adsorption mechanism of doxorubicin anticancer drug on the pristine and functionalized single-walled carbon nanotube surface as a drug delivery vehicle: A DFT study, *Journal of Molecular Liquids* (2020), https://doi.org/10.1016/j.molliq.2020.114890

Theorical investigation of adsorption mechanism of Doxorubicin anticancer drug on the pristine and functionalized single-walled carbon nanotube surface as a drug delivery vehicle: A DFT Study

Sina Karimzadeh[1,*], Babak Safaei[2,†], Tien-Chien Jen[1,‡]

[1]Department of Mechanical Engineering Science, University of Johannesburg, Gauteng, 2006, South Africa
[2]Department of Mechanical Engineering, Eastern Mediterranean University, Famagusta, North Cyprus via Mersin 10, Turkey

Abstract

In this work, interaction and bond properties of anticancer drug doxorubicin (DOX), (6,6) armchair single-walled carbon nanotube (SWCNT), and hydroxyl- and carboxyl-functionalized SWCNT (*f*-SWCNT) have been investigated based on DFT theory to design, improve and expand carbon nanotube (CNT) drug carriers which is applied in biomedical systems such as drug delivery systems. Geometrical, structural, electrical, bonding and thermodynamic properties as well as optimized geometry, adsorption energies, quantum molecular descriptors, topological parameters and frontier molecular orbitals of different drug arrangements on CNT at the highest equilibrium at WB97XD/6-31+G (d, p) level of theory at aqueous and gas phases were explored. Our calculations showed that hydrogen bonds between active sites of DOX molecules and hydroxyl- and carboxyl-functionalized CNTs played a more important role than those with pristine CNTs in the adsorption and fixation of the studied complexes as well as their thermodynamic energy. Using quantum theory of atoms in molecules (QTAIMs) method, intermolecular interactions and corresponding parameters at critical bonding points in aqueous and gas phases were also investigated. Evaluation of the results obtained from the natural bond orbital (NBO) analysis showed that the direction of electron movement was generally from drug molecule to CNT.

Keywords: Functionalized carbon nanotube; Doxorubicin; Drug delivery system; Density functional theory; QTAIM; NBO

1. Introduction

In the recent decade, extensive attention has been paid to carbon nanotubes (CNTs) and its applications on different industries due to their superior mechanical properties such as tensile and stress strengths and elasticity [1,2], as well as unique chemical and thermal properties [3]. Due to their intrinsic properties and high dynamism, they have been recently applied as drug adsorbers in medical

* E-mail: skarimzadeh@uj.ac.za
† Corresponding Author. E-mail: babak.safaei@emu.edu.tr (Babak Safaei)
‡ Corresponding Author. E-mail: tjen@uj.ac.za (Tien-Chien Jen)

and pharmaceutical industries [4–6] Furthermore, due to their characteristic surface properties and capsule and needle like shape, they can encapsulate a variety of biomolecules such as drugs and DNA molecules. They can also vertically pierce and penetrate cell membrane through endocytosis process [7] and, as carriers, protect their payloads against environmental hazards or prevent the unwanted distribution of anticancer drugs until reaching the target site in body tissues. It is noteworthy that, pristine CNTs are highly hydrophobic and their most important disadvantage in biological and pharmaceutical chemistry is their weak solubility and dispersibility, which can result in the accumulation of these compounds by Van der Waals interactions in aqueous environments. This accumulation is not favorable in drug delivery system (DDS) systems since it increases their size and therefore, decreases their ability to pierce cell membrane, resulting in the increase of their toxicity and decrease of their dispersibility in blood [8,9].

Many research works have been performed on the application of different carbon nanotube structures such as CNTs, fullerene, graphene sheets and graphene oxide in drug delivery systems [10–12]. CNTs, fullerene and graphene sheets have high surface areas which can be engineered. For example, they can be precisely fabricated and functionalized through different methods such as chemical vapor deposition (CVD), acid washing and atomic layer deposition (ALD) [13–15]. A great amount of research has been conducted to functionalize carbon atoms using different techniques to solve CNT defects and issues [16,17]. Among the most important applications of ALD in medical industry, are medical biosensors, drug delivery, and gas detection sensors [18] fabricated using very accurate layer by layer coating technique. Also, they are of great importance in today's research areas to reinforce body implants and make them biocompatible to physiological conditions of the body by making them resistant to erosion and oxidation. Recently, Zhu *et al.* [19] studied the functionalization of titanium implants reinforced with CNT and chitosan composite using ZnO particles deposited by using ALD method to improve its antibacterial properties.

CNTs can create noncovalent and covalent $\pi - \pi$ interactions with molecules via their outer and inner cavity surfaces [20]. Functionalization of CNT surface with hydrophilic atoms can solve accumulation problems. Hydrogen bonding interactions for engaging a drug compound has been shown previously which is effective in applications such as modification of drug properties as well as evaluation, identification and delivery of drugs [21,22]. This can also improve drug release control, bioavailability, performance, sensitivity and biocompatibility of the carriers and decrease their pharmacological toxicity. Therefore, functionalization is widely being used to expand carbon-based nano-carriers. Also, recent studies have been performed using –COOH functionalized CNTs on the filtration and elimination of toxic pollutants acrolein and acrylamide from cigarette smoke [23,24].

CNTs are promising DDS carriers to extend drug release duration and accumulate drugs at tumor site by improving their infiltration. The bonding strength of drug molecules with CNTs and the amount of drug release may be different at different pH values [25]. DOX is a chemotherapy drug and a anthracycline cytostatic antibiotic with molecular formula $C_{27}H_{29}NO_{11}$. This drug is applied in the treatment of different types of cancers such as breast, stomach, thyroid, bladder, bone, lung, muscle, neural tissue, joint and soft tissue cancers. It is also applied for treating Hodgkin's diseases and different types of blood cancer [26].

DOX is intercalated between base pairs in DNA helical structure and blocks DNA replication for protein synthesis. It also decelerates or blocks the growth of cancer cells through deactivating topoisomerase enzyme II, which is vital for the growth and division of cells. DOX is toxic and, along with cancer cells, can damage healthy cells in bloodstream [27]. Hence, nano-carriers can greatly improve the application of chemotherapy drugs and reduce their damage to non-cancerous cells. Due to the application of nanotechnology, new DDS systems can decrease the amount of the released drug and perform drug delivery function in a controlled manner, they protect drug molecules and due to their very small size, they can easily pass through biological barriers and deliver the drug at target point and also increase biocompatibility [28]. Due to their intrinsic properties, CNTs can act as suitable drug carriers to deliver toxic anticancer drug DOX to decrease its side effects [29]. Other nano-carriers of DOX, such as liposome, dendrimer, fullerene, metal oxide particles, biocompatible chitosan polymers and polyethylene glycol, have also been applied [30–32]. Different nanocomposite carriers have also been applied to deliver DOX molecules [33]. Due to their metallic and semi-conductive properties, carbon-based nano-structures have high potential to be used as sensors in nano-scaled devices. They can be also applied in gas detection sensors and biosensors [34]. Due to their unique electronic properties, CNTs can react well with different gas and biomolecules. For example, attaching Pd atom onto CNT surface can improve the interaction of gas molecules with CNT surface and therefore the sensitivity of these sensors [35]. Also, in another work, Pd-doped SWCNT and phenylalanine were used as high-sensitivity nanoreceptors [36]. San *et al.* [37] applied suspended carbon nanotube (SWCNT) as biosensor for the detection of DNA. Furthermore, recent DFT calculations have confirmed interactions among SWCNT and Lomustine, Ifosfamide and Droxidopia drug molecules [38–40].

The main aim of this work was to investigate the ability of pristine and hydroxyl- and carboxyl-functionalized CNTs in the adsorption of DOX and the effects of aqueous and gas phases on this process using DFT theory. Unlike other works which generally study only one certain functional group, in this work the overall effects of –COOH and –OH functional groups attached to nanotube on the adsorption of DOX molecules under similar conditions and using the same calculation method has

been investigated and the obtained results have been compared to those obtained by the same process using pristine CNTs. In the initial combination of these systems, drug molecules at their most stable state were arranged at different locations on CNT surface such that they can spontaneously be adsorbed onto and interact with CNT surface via its active atom. Our goal in performing more detailed studies on these interactions was to investigate structural properties before and after adsorption and obtain the energies of bonding, adsorption and deformation in gas and aqueous phases. To more precisely understand the nature of bonds, quantum theory of atoms in molecules (QTAIM) and topological parameter calculations were performed. Electronic properties and corresponding descriptors were obtained in both phases and the differences of pristine and functionalized CNTs were analyzed. We also performed thermodynamic, enthalpic, PDOS and TDOS analyses on adsorption process and fragments. Finally, using the natural bond orbital (NBO) method, investigated the amount and direction of charge transfer from active orbitals of CNT and drug molecules.

2. Theoretical details

Quantum mechanics calculations

DFT theory is a powerful tool for defining intermolecular interactions which are of great importance in chemical reactions and are used in the calculation of bandgap, electronica properties in semiconductors, and atomic and molecular orbital properties and energies [41]. In the current work, the interaction of hydroxyl- and carboxyl-functionalized armchair (6, 6) SWCNT and DOX anticancer drug in aqueous and gas phases has been studied. The effect of water solvation on interaction nature was evaluated using self-consistent reaction field (SCRF) implicit water with constant dielectric coefficient ε=78.3553 corresponded to Tomasi's polarizable continuum model (PCM) [42,43]. All calculations were performed based on DFT method at WB97XD/6-31+G(d,p) special level. WB97XD level of theory is very popular for NT structures and is classified as a novel DFT function category, known as range-separated function, which can capture both long- and short-rang interactions and describe charge transfer systems more precisely [44–46]. 6-31+G(d,p) basis set was suitable for general calculations of molecules with medium to huge sizes, accurate energy and properly describe core and valence orbitals, chemical bonds, long range interactions and polarization function [41]. (6, 6) pristine CNTs, which were applied in CNT functionalization, contained 132 carbon atoms with their open ends saturated with hydrogen atoms.

Gaussian is one of the powerful tools in the prediction of the properties of molecules as well as their reactions mechanism, bond energies, molecular orbitals, atomic charges, electronegativity and thermochemical properties and was therefore applied in this work. The geometry of fully optimized structures and all computations were performed using Gaussian 09 software package [47].

All DFT calculations were performed under environmental conditions of 298.150 K and 1 atm. For the characterization of DOX-nanotubes interaction, adsorption energy (E_{ads}) of the complexes were obtained using the following equation:

$$E_{ads} = E_{CNT/DOX} - (E_{CNT} + E_{DOX}) \quad (1)$$

where E_{DOX}, E_{CNT} and $E_{CNT/DOX}$ are total electronic energies of isolated DOX drug, isolated CNT and optimized DOX/CNT complex, respectively.

Boys-Bernardi counterpoise technique was employed to correct binding energies for basis set superposition error (BSSE) [48]. BSSE was determined using counterpoise (CP) method. Adsorption energy includes deformation (E_{def}) and interaction (E_{int}) energy contributions, both of which occur during adsorption. The following equations were employed for the calculation of these contributions:

$$E_{ads} = E_{int} + E_{def} \quad (2)$$

$$E_{int} = E_{CNT/DOX} - (E_{CNT\ in\ complex} + E_{DOX\ in\ complex}) \quad (3)$$

$$E_{def} = E_{def\ CNT} + E_{def\ DOX} \quad (4)$$

where $E_{CNT/DOX}$ is the total energy of optimized CNT/DOX complex and $E_{DOX\ in\ complex}$ and $E_{CNT\ in\ complex}$ are total energies of drug fragments and nanotubes in the final optimized geometry of CNT/DOX complexes, respectively. Also, $E_{def\ DOX}$ and $E_{def\ CNT}$ are the deformation energies of DOX and nanotube molecules in the complex, respectively.

To better understand the nature of interatomic interactions based on electron density distributions for detecting bond critical points (BCP) and calculating their values through of Laplacian ($\nabla^2\rho$) values and electron densities (ρ), Bader's QTAIMs has been adopted in this work [49–51]. QTAIM calculations were performed using AIM2000 software [52]. Wiberg bond index (WBI) was stated as [53,54]:

$$WBI = \sum_k P_{jk}^2 = 2P_{jj} - P_{jj}^2 \quad (5)$$

where P_{jj} and P_{jk} are charge densities in atomic orbital and density matrix elements, respectively. Higher values of WBI meant stronger covalent characters and had close correlation to bond order. Intermolecular HB energies (E_{HB}) were calculated using Espinosa method [55–57]. This method

assumed a simple relationship between potential energy density (V_{BCP}) and E_{HB} energy at a critical point corresponding to intermolecular HB contact as:

$$E_{HB} = 1/2 \; V_{BCP} \quad (6)$$

Total local energy density at BCP was stated as [58]:

$$H_{BCP} = G_{BCP} + V_{BCP} \quad (7)$$

In the above equation, V_{BCP} and G_{BCP} are local potential and kinetic energy densities at BCP, respectively.

To better understand simultaneous adsorption process of DOX molecules onto NTs, thermodynamic properties will be studied in future works.

The Gibbs free energy function [59], of a system at constant temperature was defined as:

$$\Delta G = \Delta H - T\Delta S \quad (8)$$

where the variations of Gibbs free energy (ΔG), entropy (ΔS), and enthalpy (ΔH) of all complexes at 1 atm and 298 K were determined to describe adsorption process.

The investigation of electronic properties included molecular orbitals (MO) including lowest unoccupied molecular orbital (LUMO) and highest occupied molecular orbital (HOMO) were also, calculated for the valuated systems. The gaps in the energy levels (E_g) of a system was calculated as:

$$E_g = E_{LUMO} - E_{HOMO} \quad (9)$$

Also, we calculated quantum molecular descriptors such as electronic chemical potential (μ) [60], energy gap (ev), dipole (μ) (debye), electronegativity (X) [61], global softness (s), global hardness (η) [62], and electrophilicity index (ω) [63] of NTs, DOX and evaluated complexes to describe the chemical reactivity and stability of different configurations using the following equations:

$$\mu = (E_{LUMO} + E_{HOMO})/2 \quad (10)$$

$$\eta = (E_{LUMO} - E_{HOMO})/2 \quad (11)$$

$$\omega = \mu^2/2\eta \quad (12)$$

In this work, the thermodynamic and kinetic aspects of the interaction between NTs (i.e., the acceptor, A) and DOX (i.e., the donor, B) have also been studied. The global NTs-DOX interaction can be calculated using ΔN parameter which shows the fractional number of electrons transferred from fragment B (donor) to fragment A (acceptor) and elucidate component stability; this factor can be calculated as:

$$\Delta N = \frac{(\mu_B - \mu_A)}{(\eta_A + \eta_B)}$$

(13)

where η and μ are the chemical hardness and potential of acceptor (A) and donor (B), respectively.

Positive values of ΔN indicate that charge was transferred from B to A and A acted as electron acceptor, while negative values of ΔN indicated that charge was transferred from A to B and A acted as electron donor. Sarmah *et al.* [64] proposed comprehensive decomposition analysis of stabilization energy (CDASE) method and found that stabilization energy (SE) and its different components as well as charge transfer can be employed to find the most stable adduct obtained by noncovalent interactions [65,66]. Overall stabilization energy could be expressed as:

$$\Delta E_{SE(AB)} = \Delta E_{A(B)} + \Delta E_{B(A)} = -\frac{(\mu_B - \mu_A)^2}{2(\eta_A + \eta_B)}$$

(14)

where η_A and $\mu_A$are the chemical hardness and potential of acceptor (A), respectively. Similarly, and indicate the same parameters for the donor (B). The changes of individual energy components (i.e., $\Delta E_{A(B)}$ and $\Delta E_{B(A)}$) are stated as:

$$\Delta E_{A(B)} = \frac{(\mu_B - \mu_A)}{(\eta_A + \eta_B)}\left[\mu_A + \frac{1}{2}\eta_A\left(\frac{\mu_B - \mu_A}{\eta_A + \eta_B}\right)\right] = \Delta N\left(\mu_A + \frac{1}{2}\eta_A \Delta N\right)$$

(15)

$$\Delta E_{B(A)} = \frac{(\mu_B - \mu_A)}{(\eta_A + \eta_B)}\left[-\mu_B + \frac{1}{2}\eta_B\left(\frac{\mu_B - \mu_A}{\eta_A + \eta_B}\right)\right] = \Delta N\left(-\mu_B + \frac{1}{2}\eta_B \Delta N\right)$$

(16)

Density of states (DOS) of a system shows state number in the intervals of unit energy. In an isolated system, energy levels are discrete, and the concept of DOS is not clear. However, if discrete energy levels are artificially expanded to the curve, DOS diagram can act a powerful tool to describe the composition of orbitals [67–69]. The curve of partial density of states (PDOS) can be applied to visualize orbital compositions. PDOS function of fragment A can be stated as:

$$PDOS_A(E) = \sum_i E_{i,A}\, F(E - \varepsilon_i)$$

(17)

where $E_{i,A}$ is the composition of orbital i and fragment A and ε_i shows single-particle Hamilton eigenvalue set [70]. Visualization of PDOS spectra was performed by Multiwfn 3.6 software [71] using the data obtained from WB97XD/6-31+G(d, p) level of theory.

3. Results and Discussion

3.1 DFT Results

3.1.1 Molecular Geometry and Binding Energy Analyses

To obtain the configuration with the highest stability, the interactions of DOX molecule with CNT and *f*-CNTs as drug carriers at various positions have been studied. Following structural optimization, drug molecule re-arrangements in some configurations were predicted to find the most stable configuration. Figs. 1 and 2 show the optimized geometries of anticancer drug DOX, CNT, and *f* -CNTs as well as the most stable DOX/NTs complexes with their corresponding atom numbers.

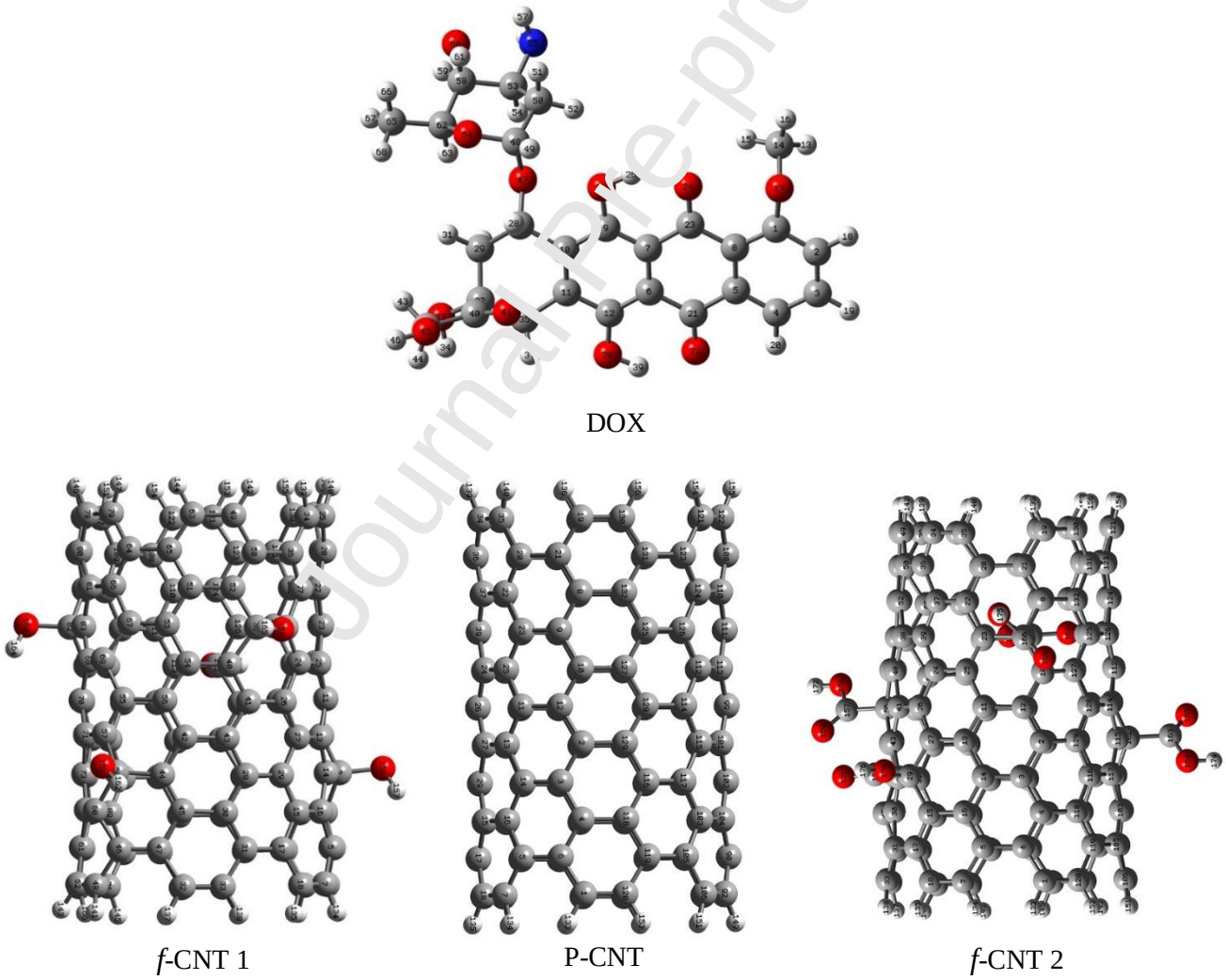

DOX

f-CNT 1 P-CNT *f*-CNT 2

Fig. 1. The optimized geometries of DOX, Hydroxylated (*f*-CNT1), pristine CNT (PCNT) and Carboxylated (*f*-CNT2)

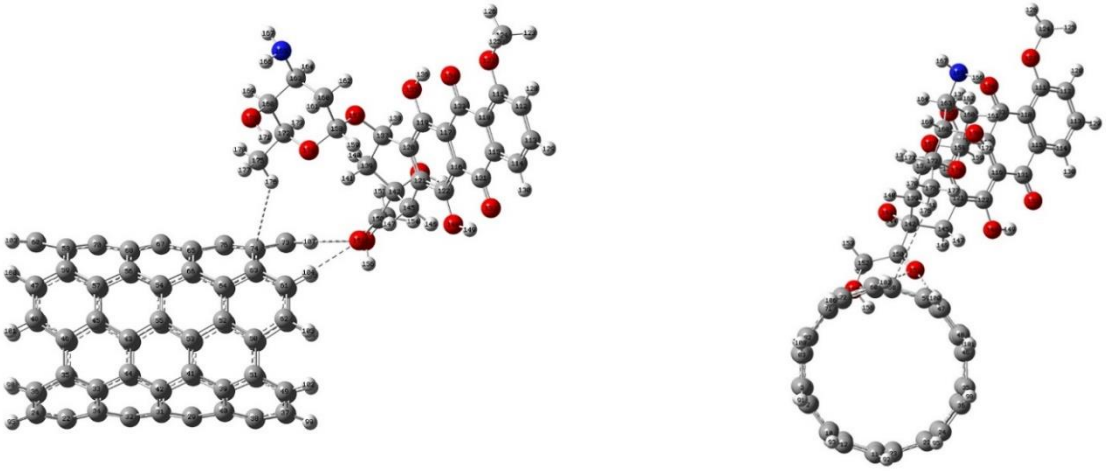

(A)

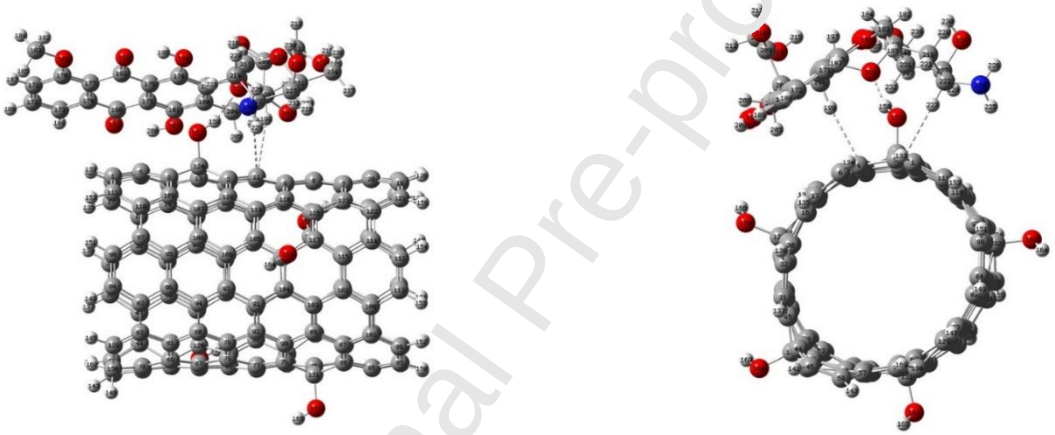

(B)

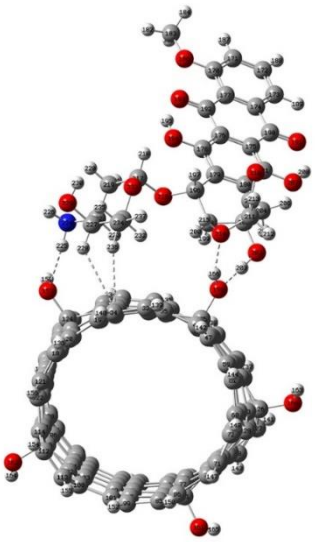

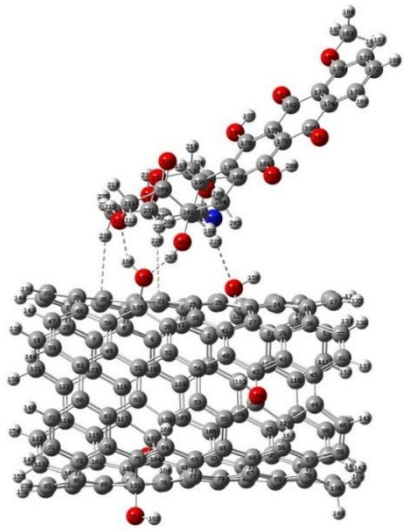

(C)

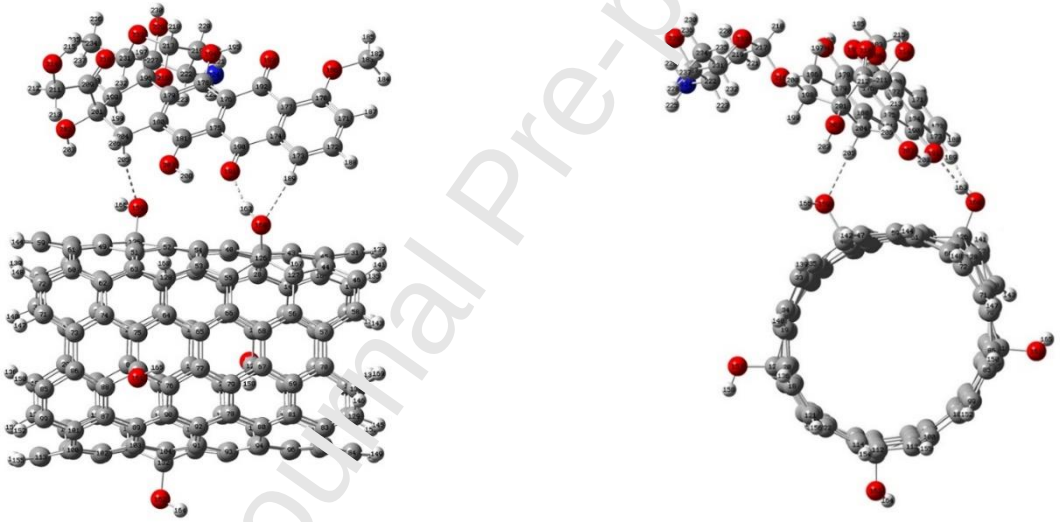

(D)

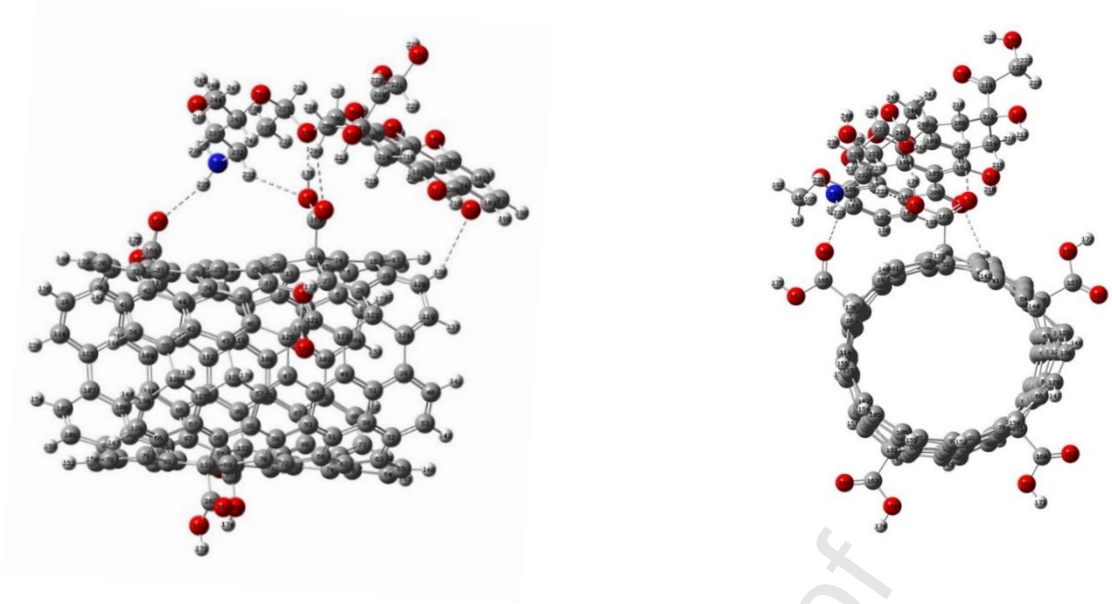

(E)

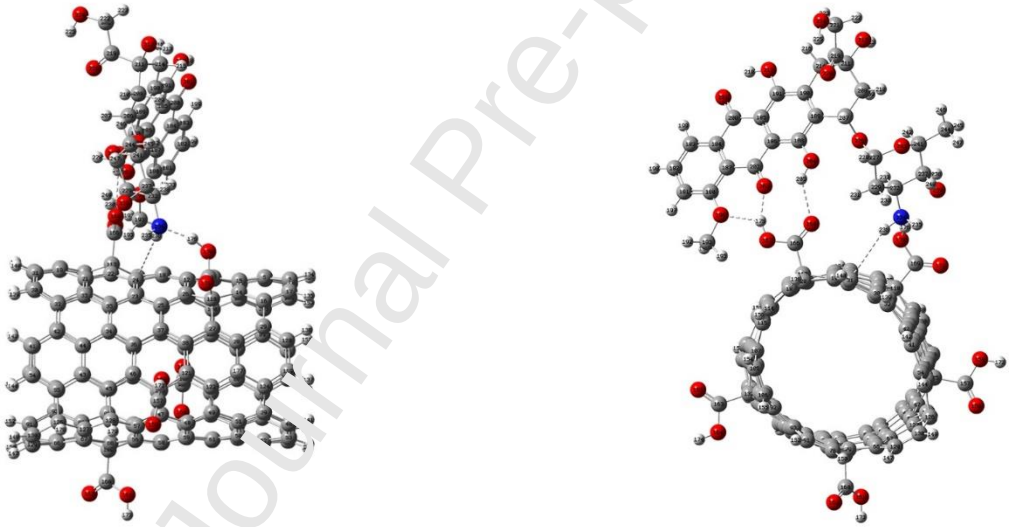

(F)

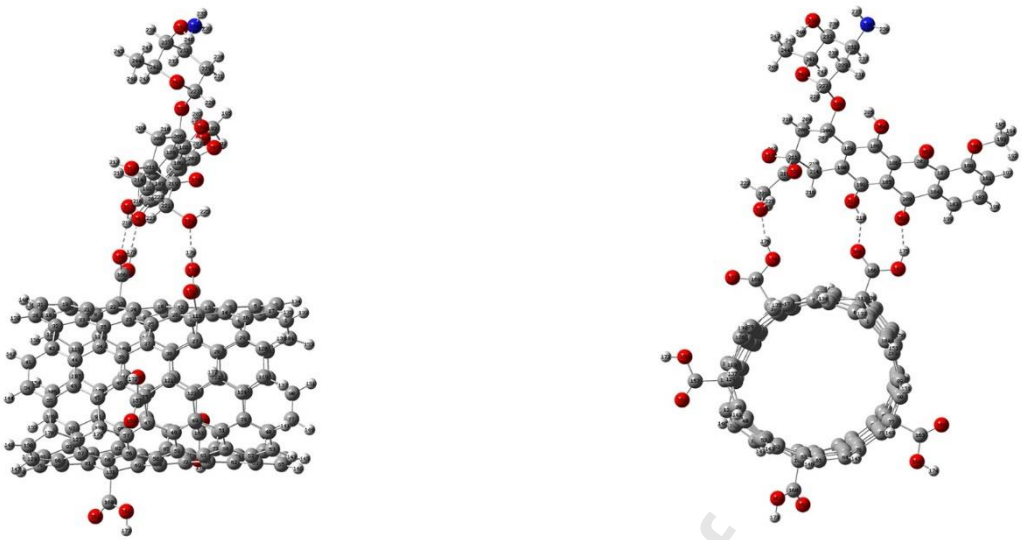

(G)

Fig. 2. Final optimized geometries of DOX/NTs complexes at the most stable state of energy, calculated by WB97XD/6-31+G (d, p) method (A: complex with pristine CNT; B, C and D: complexes with hydroxylated CNT; E, F and G: complexes with carboxylated CNT). Corresponding color for atoms were: carbon in grey, oxygen in red, hydrogen in white and nitrogen in blue.

The geometries of pristine, carboxylated and hydroxylated armchair (6,6) CNTs with diameter 8.5 Å, length 14 Å and two saturated ends applied as nano vectors for the adsorption of DOX were totally optimized at the WB97XD/6-31+G (d, p) level of theory. Table 1 lists some critical bond angles and lengths. The lengths of optimized P-SWCNTs before and after adsorption were calculated to be 14.02 Å and 11.57Å, respectively. However, the nanotube lengths in other complexes of *f*-CNT were fixed at 14 Å. Table 2 lists the structural parameters of DOX before and after being adsorbed onto the surface of nanotubes with selected configurations (i.e. A, B, E). Also, analyzing structural parameters at 6-31+G (d, p) indicated that drug molecule bond lengths in the considered complexes remained almost constant with respect to WB97XD functional (Table 2). However, no significant perturbation was witnessed in the relaxed geometry of DOX molecules after being adsorbed onto the surface of nanotubes with the studied configurations. One could conclude that nanotubes acted as drug carriers and protected DOX molecules from degradation. These results proved that CNT had great potential as a safe nanocarrier for DOX molecules in DDS systems.

Table 1. Some critical bond angles and lengths of P-SWCNT and *f*-SWCNT in PCM at considered configurations

Complex	**Bond label**	Bond length (A)		**Bond angle label**	Bond angle (degree)	
		Before ads	After ads		Before ads	After ads
A	C63-C74	1.346	1.476	C61-C63-C74	122.017	121.120
	C61-H104	1.070	1.070	C63-C61-H104	119.692	120.227

B	O158-H158	0.970	0.980	C124-O157-H158	109.737	114.928
	C124-O157	1.446	1.439			
E	C169-O170	1.341	1.324	O170-C169-O171	123.114	124.641
	O170-H176	0.971	1.004	C169-O170-H176	113.026	117.084
	C169-O171	1.204	1.211			
	C118-C169	1.533	1.531			

Table 2. Structural parameters of DOX before and after being adsorbed onto NT in (CONF A, B, E) in PCM

Bond label	Bond length (Å)				**Bond angle label**	Bond angle (degree)			
	Before ads	After ads				Before ads	After ads		
		CONF-A	CONF-B	CONF-E			CONF-A	CONF-B	CONF-E
N55-H56	1.007	1.008	1.007	1.008	H56-N55-H57	109.60	109.64	109.79	109.70
N55-H57	1.008	1.008	1.008	1.008	C48-O47-C27	117.52	119.29	115.61	117.54
O47-C48	1.422	1.421	1.436	1.438	C32-O33-H34	111.73	112.19	108.47	111.41
O47-C27	1.448	1.446	1.458	1.464	C12-O38-H39	111.22	111.24	111.23	111.47
C32-O33	1.439	1.435	1.433	1.436	H36-C35-H37	107.54	107.32	107.47	108.26
O33-H34	0.968	0.967	0.973	0.967	C1-O17-C14	122.20	122.20	122.18	117.84
O38-H39	0.977	0.977	0.977	0.976	C9-O25-H26	110.54	110.50	110.53	110.93
C12-O38	1.356	1.356	1.357	1.355	H43-C42-H44	107.42	107.89	108.71	107.99
C21-O22	1.232	1.232	1.232	1.235	C40-C42-O45	107.43	110.89	111.97	109.83
C35-H36	1.085	1.081	1.083	1.083	C21-C7-C23	119.42	119.37	119.39	119.40
C35-H37	1.081	1.082	1.079	1.080	C62-O64-C48	114.38	113.90	114.54	114.75
C4-H20	1.068	1.068	1.068	1.068	O33-C32-C40	109.15	109.99	110.01	104.12
C1-O17	1.350	1.350	1.351	1.372					
O17-C14	1.450	1.450	1.450	1.426					
C23-O24	1.231	1.231	1.231	1.233					
C9-O25	1.356	1.354	1.355	1.355					
O25-H26	0.979	0.979	0.980	0.979					
C40-O41	1.211	1.216	1.212	1.216					
O45-H46	0.966	0.967	0.966	0.970					
C5-C8	1.399	1.398	1.398	1.399					

3.1.2 Analysis of Binding Energy

Tables 3 lists the deformation (E_{def}) interaction (E_{int}) and adsorption (E_{ads}) energies of the studied systems in aqueous and gaseous phases calculated through Eqs. (1) to (4). The calculated binding energy values for pristine SWCNT complex were -4.637 and -6.390 Kcal/mol and corresponding values for hydroxylated CNT complexes (i.e. B, C, and D) ranged from -13.796 to -17.829 Kcal/mol and -18.859 to -33.022 Kcal/mol and for carboxylated CNT complexes from -33.508 to -39.978 Kcal/mol and -40.549 to -43.674 Kcal/mol in aqueous and gaseous phases, respectively. Research findings have shown that the ebsorption power between nanotube surface and DOX molecule was weak [72-74]. Higher values of absorption energy in aqueous solution indicated higher absorption powers which seemd to be overestimated when compared with real values. The reason for this overestimation could be the selection of implicit water model for calculations where in the model,

the reaction between complex fragments and water molecules was cont considered as real [75, 76]. However, this model predicted acceptable comparative data in terms of absorption power among studied structures.

Based on the final optimized structures, Fig. 2 shows that, due to low bonding energies, unlike functionalized CNT, in pristine CNT drug molecules do not directly bond to CNT surface and are adsorbed onto CNT terminal after rotation and displacement and tend to be encapsulated within the cavity which was inconsistent with the results obtained from dynamic simulation in our previous work [77]. It was found that the binding energies of all appropriate structures in aqueous media were lower than the values obtained in gaseous phase. It was also found that, the calculated binding energies were negative in all cases, which indicated that adsorption process was exothermic and favorable in both phases in the majority of the evaluated systems (Tables 3). In addition, considering the results given in Tables 3, it was found that binding energies were mainly under the influences of the orientations and locations of DOX molecules. Also, our theoretical calculations revealed a good relationship between the E_{int} and E_{ads} in adsorption structures. It was also concluded that increase of interaction energy shifted binding energies toward more negative values making intermolecular interactions stronger. Further, the contribution of interaction energy in the evaluated configurations (Table 3) confirmed that DOX molecules were physiosorbed onto the surface of NTs.

Following optimization, pristine CNT complex (A), (Fig. 2) presented negative binding energies -4.637 and -6.390 Kcal/mol in aqueous and gaseous phases, respectively. In the configuration with the highest stability, one Van der Walls (VdW) interaction between carbon atom C74, CNT surface and H176 atom of drug molecule was formed with distances of 3.319 and 3.673Å in PCM and gas phases, respectively. Also, a weak H bond was formed between H104 atom of CNT in terminal and O151 atom of DOX with intermolecular O…H distances of 2.339 and 2.342 Å in PCM and gas phases, respectively. These values proved the presence of VdW interactions between P-SWCNT and DOX drug molecules. They also indicated that the strengths of P-SWNTs-DOX interaction was very weak. To enhance binding strengths, the electronic and structural characteristics of SWCNT, -COOH and -OH functional groups were attached onto the exterior surfaces of nanotubes (f-SWCNTs).

After optimizing hydroxylated CNT (f-CNT1) complexes (i.e. B, C, and D complexes), the intermolecular distance from DOX to f-CNT1 surface was in 1.624-2.313Å range and configuration C was found to be the most stable structure (Fig. 2) and therefore it had the most negative binding energies in aqueous and gaseous phases; i.e. -17.829 and -33.022 Kcal/mol, respectively. In this configuration, 3 hydrogen bonds were formed on nanotube surface. In aqueous phase, one hydrogen bond was created through the interaction of H166 atom of -OH group on the surface of CNT and O214 atom of DOX molecule (DOX molecule was diagonal to CNT surface) with intermolecular O…H

distance of 1.777 Å. The second hydrogen bond, which was common in both phases, was formed through the interaction of O159 atom of -OH group on CNT and H203 atom of DOX with intermolecular O…H distances of 1.654 and 1.783 Å in PCM and gaseous phases, respectively. Finally, the third hydrogen bond was formed in gas phase through the interaction of H158 atom of -OH group on CNT and N224 nitrogen atom of DOX with intermolecular N…H distance of 1.826 Å, (DOX molecule was parallel to CNT surface). It should be kept in mind that the binding with the most negative energy, which was formed between hydroxylated *f*-CNT1 and DOX molecule in configuration C, was because of more intermolecular hydrogen bond (HB) interactions. Following configuration C, configuration D had the most stable state among hydroxylated CNT configurations with binding energy of -16.040 and -29.645 Kcal/mol in aqueous and gaseous phases, respectively. At the most stable state, this system had two dominant hydrogen bonds. The first one was formed between O191 oxygen atom of carbonyl group on DOX molecule and H163 hydrogen atom from the hydroxyl functional group on CNT surface with bond distances of 1.823 and 1.903 Å in aqueous and gaseous phases, respectively. The second bond was formed between O159 oxygen atom of *f*-CNT1 and H203 hydrogen atom of DOX with intermolecular distances of 1.903 Å.

In configuration B, a hydrogen bond was formed between H158 hydrogen atom of hydroxyl group on the surface of CNT and O216 oxygen atom of DOX with bond distances of 1.825 and 1.798 Å in aqueous and gaseous phases, respectively. Weak VdW bonds were formed between H233 hydrogen atom of drug molecule and H199 hydrogen atom on CNT surface. In final optimization of the system, aromatic rings of DOX were arranged along CNT axis. After optimizing carboxylated CNT (*f*-CNT2) complexes, the intermolecular distances of *f*-CNT2 surface and DOX molecule were in 1.573-2.496 Å range with configuration F being the most stable structure (Fig. 2) which had the most negative binding energies of -39.978 and -43.674 kcal/mol in aqueous and gaseous phases, respectively. In the configuration with the highest stability, two main hydrogen bonds were formed on CNT surface. The first hydrogen bond was formed through the interaction of H175 atom of -COOH group on CNT and O203 atom of DOX (DOX molecule was perpendicular to CNT surface) with intermolecular OH distances of 1.702 and 1.698 Å in aqueous and gaseous phases, respectively. However, the second one was formed between H176 atom of -COOH group of *f*-CNT2 and N234 nitrogen atom of DOX with N…H distances of 1.672 and 1.679 Å in PCM and gas phases, respectively.

In the most stable state of configuration E, the arrangement of DOX molecule was similar to the configuration B, where O266 oxygen atom of DOX formed a dominant hydrogen bond with the hydrogen atom of carboxyl group on CNT with minimum intermolecular distance of 1.573 Å in aqueous phase in the studied system. In configuration G, DOX molecule was located 180^{o} opposite to the position of DOX molecule in complex F which resulted in the formation of three hydrogen bonds,

two of which were formed by -OH of drug molecule, i.e. O168…H218 and O224… H176 with bond distances of 1.869 and 1.633 Å and 1.766 and 1.573 Å in aqueous and gaseous phases, respectively, and the other one was formed by O201 oxygen atom of carboxyl functional group of DOX molecule and H175 hydrogen atom of carboxyle functional group on CNT surface with bond distance of 1.736 Å in both phases. Also, as given in Table 3, the deformation energies of the evaluated models were in 4.746–18.210 Kcal/mol range. The obtained results revealed that, remarkable deformation occurred in the molecular geometry of DOX during the forming some of configurations. It is well established that by the increase of the strength of interaction increases the intensity of curvatures in carriers during conjunction with DOX molecule. The results given in Table 3 show that the strength of interaction between drug and *f*-CNTs was higher than that with P-CNT. The maximum and minimum energies of deformation were found to be 18.21 and 4.746 Kcal/mol for systems E and A, respectively, which meant that the distortion in the geometry of drug and nanotube in the *f*-CNT system's is significantly higher than P-SWCNT system (Table 3).

Adsorption energy magnitude at WB97XD level of theory for the above discussed complexes was:

P-CNT<Hydroxylated CNT<Carboxylated CNT

Therefore, the obtained results revealed that the addition of -COOH and -OH functional groups onto the exterior surfaces of NTs markedly enhanced the stability of configurations and adsorption process.

Based on our theoretical findings, configurations C and D showed weaker interaction between *f*-CNT1 and DOX molecules in aqueous solutions than gas phase. More detailed investigation of the data presented in Table 3 showed that adsorption energies in complexes C and D were significantly different in aqueous and gas phases. The initial structure selected for the investigation of drug molecule adsorption on *f*-CNT revealed that DOX molecules were aligned parallel such that their aromatic rings were located on the surface of nanotubes in both phases. It was witnessed in the optimized structure of configuration C that three intermolecular hydrogen bonds were formed between the functional groups on nanotube surface and DOX molecules namely N224…H158 in gas phase, O214…H166 in aqueous phase, and O159…H203 in both phases. In configuration D, however, two intermolecular hydrogen bonds between the functional groups on nanotube surface and DOX molecules which included O159…H203 in gas phase and O191…H163 commonly in both PCM and gas phases. More detailed evaluation of the data presented in Tables 3 also revealed that intermolecular hydrogen bond (HB) interactions in aqueous phase were weaker than those occurring in gas phase. In gas phase, stronger intermolecular interactions were formed between *f*-CNT and DOX

molecules. So, the adsorption energy of functionalized nanotubes and drug molecules was greatly improved in gas phase.

According to the results obtained in this section, it could be concluded that, intermolecular hydrogen bonds have important role in the stability of physisorption, also can be useful in developing carbon nanocarriers for DOX and on the basis of target environmental conditions, i.e. pH of target medium, suitable samples can be used for DDS systems to optimize drug release conditions. Also, other nanocarrier structures such as multi walled carbon nanotube and hybrid CNT-polymer could be used to improve drug encapsulation capability [78,79].

Table 3. The calculated adsorption energy (E_{ads}), interaction energy (E_{int}) and deformation energy (E_{def}) (all in Kcal/mol) in DOX/CNT and DOX/f-CNT systems for all complexes

MODEL	E_{int}	E_{ads}		E_{def}
		PCM	GAS	
A	-11.136	-4.637	-6.390	4.746
B	-31.851	-13.796	-18.859	12.992
C	-47.902	-17.829	-33.022	14.880
D	-46.126	-16.040	-29.645	16.481
E	-59.271	-38.508	-41.060	18.210
F	-59.664	-39.978	-43.674	15.990
G	-54.595	-37.470	-40.549	14.046

3.1.3 QTAIM Analysis

It can be seen in Fig. 2 that, in the studied complexes, oxygen, nitrogen and hydrogen atoms in DOX molecules formed bonds with oxygen, carbon and hydrogen atoms in CNTs and f-CNTs. Hence, the studied structures were stabilized by various intermolecular HB interactions. To study this fact in more detail, intermolecular HB energies (E_{HB}) were calculated using Espinosa method, as summarized in Table 4. As given in Table 4, DOX molecules could participate in a wide range of intermolecular conventional (N-H…O, N…O-H, O…O-H and O-H…O) and nonconventional (H…C and O… H) HBs with NTs.

The results listed in Table 4 reveal that E_{HB} values for O…H, O-H…N, O…H-N, and O-H…O in systems containing f-CNTs were considerable. Detailed evaluation of C and E complexes in systems containing f-CNT1 and f-CNT2, respectively, revealed that the magnitude of HB interaction is more than complex A with non-functionalized surface. Hence, one could conclude that HB interaction was among the most important factors in the stability of the studied complexes.

To better understand the nature of intermolecular interactions between CNT and DOX molecules, QTAIM calculation was applied. This theory analyzes the electron density of various characteristic points, especially bond critical points (BCPs), to obtain electron density (ρ_{BCP}) and Laplacian ($\nabla^2_{\rho_{BCP}}$) values to determine the strength and characteristic of bonds, respectively. Table 4 lists the values of kinetic electron density (G_{BCP}), local potential electron energy density (V_{BCP}), total electron energy density (H_{BCP}), Laplacian ($\nabla^2_{\rho_{BCP}}$), and electron densities (ρ_{BCP}) for all structures.

Table 4. The topological parameters, Lagrangian kinetic (G_{BCP}) and potential (V_{BCP}) electron energy densities (all in a.u.), Laplacian ($\nabla^2\rho_{BCP}$), electron density(ρ_{BCP}), total electron energy density (H_{BCP}) along with its two components, hydrogen bond energy (E_{HB}, in Kcal/mol), and intermolecular distance (R) in (Å) for intermolecular interactions between DOX and NTs in the considered complexes in aqueous solution, calculated using Espinosa method

Model	Bond	ρ_{BCP}	$\nabla^2\rho_{BCP}$	G_{BCP}	H_{BCP}	V_{BCP}	E_{HB}	R
A	H104…..O151	0.009921	0.014423	0.011438	0.002986	-0.00845	-2.652	2.339
	H107…..O155	0.010605	0.014668	0.011735	0.002934	-0.0088	-2.761	2.486
	C74…....H176	0.001286	0.001408	0.000998	0.00041	-0.00059	-0.184	3.551
B	H158….O216	0.036464	0.030016	0.038337	-0.00832	-0.04666	-14.639	1.825
	C2-C11…H223	0.008232	0.007343	0.006169	0.001174	-0.005	-1.567	2.749
	C10-C24….H199	0.006502	0.005789	0.004665	0.001124	-0.00354	-1.111	2.835
C	O159……H203	0.052766	0.033907	0.052	-0.01809	-0.07009	-21.991	1.654
	H166……O214	0.040821	0.033361	0.043307	-0.01025	-0.05385	-16.896	1.777
	H158……N224*	0.044723	0.023634	0.036023	-0.01239	-0.04842	-15.191	1.826
	O157……H225	0.014680	0.018808	0.016508	0.0023	-0.01421	-4.457	2.221
	C21…...H236	0.005458	0.005030	0.004003	0.001033	-0.00297	-0.932	2.876
	C10-C24.....H228	0.004780	0.004352	0.003436	0.000916	-0.00252	-0.79	3.032
D	H163…...O191	0.034228	0.030900	0.037444	-0.00654	-0.04399	-13.801	1.823
	O159……H203	0.028766	0.028383	0.031988	-0.00361	-0.0356	-11.168	1.903
	O160……H189	0.013044	0.015273	0.013911	0.002461	-0.01145	-3.592	2.295
	O159……H205	0.013096	0.015583	0.013528	0.002456	-0.01107	-3.473	2.313
E	H176……O226	0.063898	0.033764	0.057837	-0.02447	-0.08231	-25.824	1.573
	O171……H209	0.011311	0.013770	0.01201	0.002759	-0.00925	-2.902	2.379
	O170…...H233	0.008310	0.011406	0.008865	0.002541	-0.00632	-1.984	2.496
	O168……H235	0.010049	0.014954	0.011945	0.003008	-0.00894	-2.804	2.318
	H138…...O201	0.003298	0.005161	0.003458	0.001703	-0.00176	-0.55	2.791
F	H175……O203	0.044324	0.033581	0.04618	-0.0126	-0.05878	-18.442	1.698
	H175……O196	0.016408	0.026065	0.02295	0.003115	-0.01984	-6.223	2.126
	O168……H205	0.012512	0.018985	0.015938	0.003046	-0.01289	-4.045	2.198
	H176…...N234*	0.032019	0.025008	0.044987	-0.01998	-0.06497	-20.383	1.679
	C23-C24….H236	0.002769	0.003393	0.002444	0.000949	-0.0015	-0.469	3.117
G	O168……H218	0.040412	0.031339	0.04053	-0.00919	-0.04972	-15.599	1.766
	H175…...O201	0.040062	0.033132	0.043023	-0.00989	-0.05292	-16.602	1.736
	H176……O224	0.056356	0.032451	0.053127	-0.02068	-0.0738	-23.155	1.633

- * Represents bonds formed in gas phase

Rozas et al. [80] classified interaction character based on the value of ρ_{BCP} with $\nabla^2_{\rho_{BCP}}$ and the signs and values of $\nabla^2_{\rho_{BCP}}$ and H_{BCP} determine the nature of bonds such that $\nabla^2_{\rho_{BCP}} < 0$ *and* $H_{BCP} < 0$ indicated strong covalent bonding character, $\nabla^2_{\rho_{BCP}} < 0$ *and* $H_{BCP} > 0$ showed medium strength and partially covalent nature and $\nabla^2_{\rho_{BCP}} > 0$ *and* $H_{BCP} > 0$ indicated mainly weak electrostatic bonds character. Positive $\nabla^2_{\rho_{BCP}}$ values indicated VdW, electrostatic and HB bonds. Negative values of $\nabla^2_{\rho_{BCP}}$ indicate high electron density and concentration of charge in this nuclear region, leading to covalent bonds. If $\nabla^2_{\rho_{BCP}} > 0.1$, ionic bond is formed, if $\nabla^2_{\rho_{BCP}} \cong 0.1$ covalent bond is formed and if $\nabla^2_{\rho_{BCP}} \leq 0.01$ weak VdW hydrogen bond is formed. For bonds with covalent nature and high strength, we

would have $V_{BCP} > G_{BCP}$ which is a function of intermolecular distance R. Also, comprehensive analysis of the values of $\alpha = |\frac{G_{BCP}}{V_{BCP}}|$ revealed that when $0.1 \leq \alpha \leq 0.5$, covalent bond is formed, when $0.5 \leq \alpha \leq 1$, ionic covalent bond is formed in which covalent bond tends to be polarized and has partially ionic nature, and when $\alpha > 1$, by assuming negative values for $\nabla^2_{\rho_{BCP}}$, weak covalent bond is formed and by assuming positive values for this term, we have electrostatic bond.

Hence, calculated electron density of DOX/NTs complexes revealed that intermolecular hydrogen bonds had low and positive ρ_{BCP} in the range of (0.001 to 0.06 a.u) and $\nabla^2_{\rho_{BCP}}$ values in the range of (0.001 to 0.033 a.u) in implicit water phase. The values of $\nabla^2_{\rho_{BCP}}$ and ρ_{BCP} were in the acceptable range of HB interactions [81–83] proving the presence of closed-shell interactions in the studied complexes. Therefore, these factors with negative or positive H_{BCP} values at intermolecular H-bonding indicated that the studied complexes had electrostatic and partially covalent natures simultaneously. Our finding were in agreement with previous works [73,84,85]. Electron densities at BCPs of N…H, O…H, and C…H in DOX/f-CNT and DOX/P-CNT systems respectively, had good correlation with energy strength E_{HB}. Therefore, high electron densities corresponded to higher values of E_{HB} and vice versa (Table 4). The maximum values of electron density (ρ_{BCP}) and E_{HB} for f-CNT1 and f-CNT2 systems obtained for C and E complexes at O159…H203 and H176…O226 contact points were 0.052766 a.u, -21.991 Kcal/mol and 0.063893 a.u, -25.824 Kcal/mol, respectively. The amount of E_{HB} parameter illustrate bond strength. Generally, shorter intermolecular distance between drug atoms and surface atoms of NT's, enhance the strength of E_{HB}. The data presented in Tables 4 revealed that in complex C, the length of intermolecular O-H···H hydrogen bond between O_{159} …. H_{203} was shorter than that between H_{166} …. O_{214} and in complex F, H_{175} …. O_{203} hydrogen bond length was shorter than H_{175}…. O_{196}; therefore, shorter conjugations formed stronger H-bonds.

Also, more detailed investigation of complex F in Table 4 showed that two dominant hydrogen bonds were formed between O203 of drug and H175 of CNT as well as N234 and H176 of CNT with E_{HB} values of -18.442 and -20.383 Kcal/mol, respectively, while system E with one bond was more stable. These results complied well with those obtained in the previous section for the most stable configuration, i.e. complex F. It was concluded that higher electron densities at BCP corresponded to higher strengths of intermolecular hydrogen bonds. To emphasize this, the relationships between ρ_{BCP} and $\nabla^2_{\rho_{BCP}}$ versus E_{HB} at intermolecular interaction are determined and shown in Figs. 3 and 4, respectively. The correlation coefficients of these dependencies were very close to 0.99.

In addition, Fig. 5 shows the molecular diagrams of CNT, DOX, and selected most stable complexes C and F, which revealed the positions of all critical points and bond paths between attractors in DOX/NTs systems. Red dots on the bonds showed bonds BCP points and yellow dots

represent rings critical points in structural rings. The positions of critical points on bonds greatly depended on electronegativity and also the critical point of the bond is closer to the atom with lower electronegativity. Fig. S6 shows electron density Laplacian contour maps of all critical points in all studied complexes.

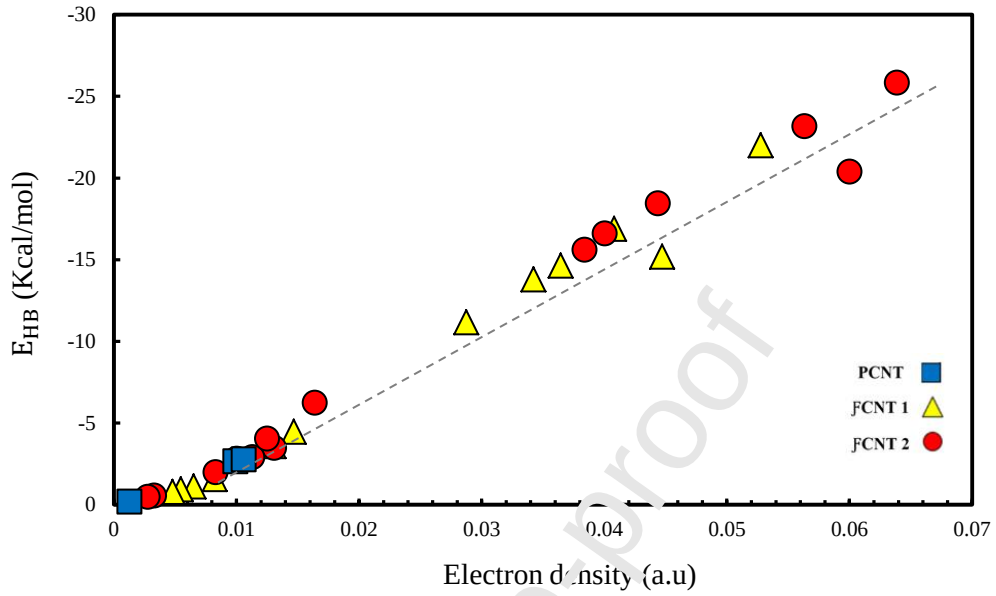

Fig. 3. Correlation between calculated ρ_{BCP} and E_{HB} energies at BCP

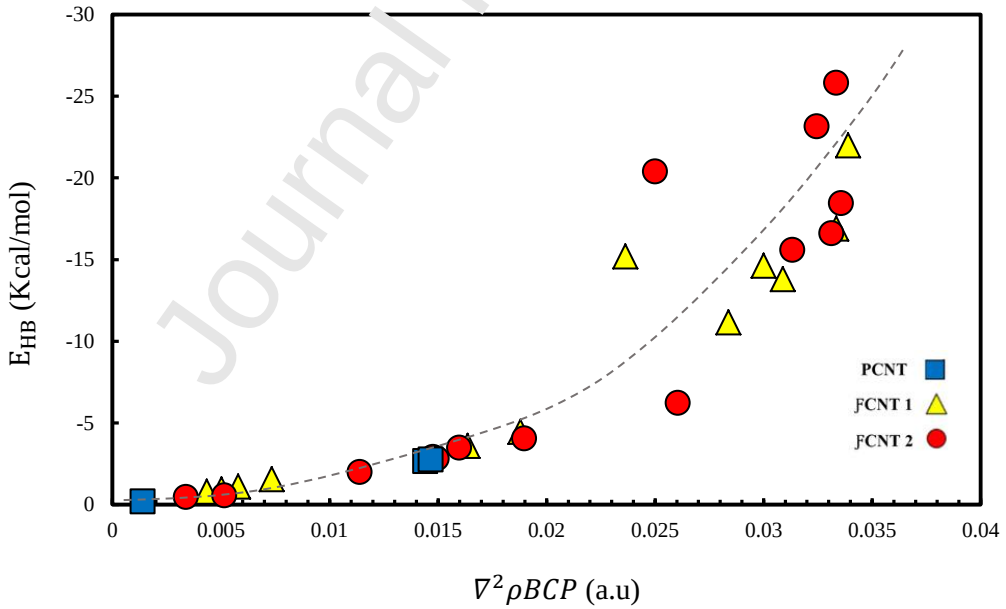

Fig. 4. Correlation between calculated $\nabla^2_{\rho_{BCP}}$ and E_{HB} energies at BCP

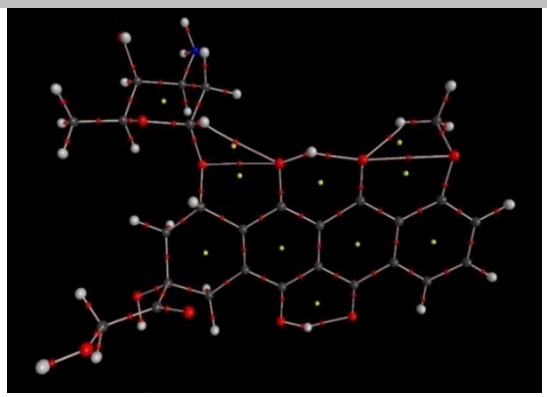

DOX

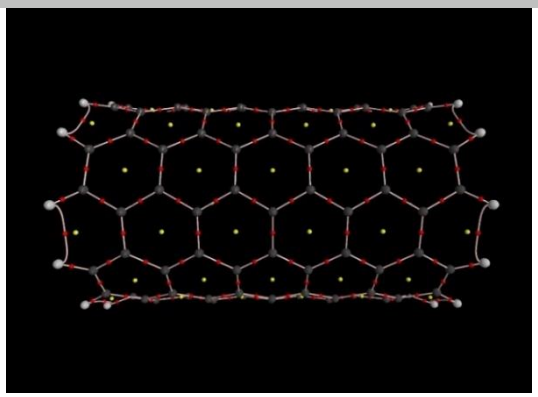

P-SWCNT

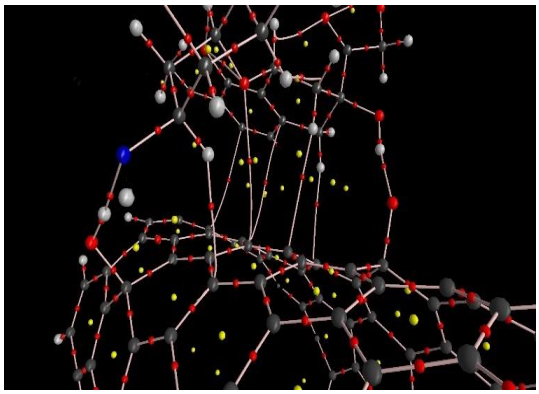

Complex C

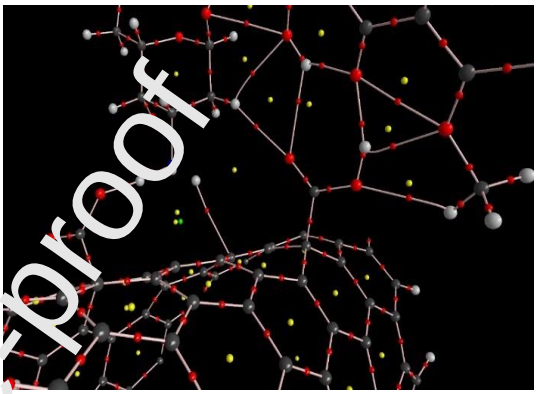

Complex F

Fig. 5. Molecular diagrams of P-CNT, DOX and the most stable complexes (C and F) obtained from DFT calculations

3.1.4 Thermodynamic Properties

For the calculation of energy, Gaussian software considers contributions of translation as well as electronic, rotational and vibrational motions and their values are obtained as the sum of electronic and thermal free energies since Gibbs free energy integrates entropy and enthalpy into one single value. Free energy variations, ΔG, could be obtained by adding the value of enthalpy to entropy-temperature product. Gibbs free energy variations is defined as Gibbs energy difference between initial (before absorption) and final (after absorption) states which is obtained using Eq. (8). Thermodynamic parameters can provide deeper understanding on essential energy changes due to adsorption; therefore, these parameters should be comprehensively investigated.

The Gibbs free energy (ΔG), entropy (ΔS), and enthalpy (ΔH) of all complexes at 1 atm and 298 K were determined to describe adsorption process in implicit water PCM (Table 5). Negative standard enthalpy or give out energy in the form of heat $\Delta H < 0$, and positive entropy or increase in the disorder of the system $\Delta S > 0$ values meant thermodynamically favorable and spontaneous formation

of E, F, G complexes in aqueous phase. On the other hand, the WB97XD level of theory predicted that adsorption process had exothermic enthalpy and, positive $T\Delta S$ values for complexes containing f-CNT2 indicated stable entropy variations during complex formation. It was found that the formation of A, B, C, and D complexes at WB97XD functional entropically was not favorable, but the quantity of Gibbs free energy ΔG which reflect the balance between two potential was negative. Therefore, concluded that the adsorption process for all studied systems was thermodynamically favorable and spontaneous. Complexes with higher values of relative standard Gibbs energy of formation were more stable while those with lower relative standard energy of formation were more unstable.

Table 5. Calculated thermodynamic properties (ΔG, ΔH, and TΔS), all in Kcal/mol

Complex	ΔG	ΔH	TΔS
A	-8.197	-12.589	-4.392
B	-24.079	-38.014	-13.935
C	-24.424	-38.290	-13.866
D	-24.779	-37.685	-12.906
E	-54.199	-69.671	15.472
F	-53.167	-67.418	14.251
G	-55.003	-69.060	14.057

3.1.5 Electronic Properties

Electrophilicity index (ω) is a key factor, and the value of this factor is high in most electrophilic systems. Electrophilicity index is weighted as a degree of the energy decrement of the chemical species because of the maximum rate of electron passing from ambience and provides insight about structural reactivity, stability and toxicity of chemical species. LUMO and HOMO iso levels of NTs and DOX are shown in Fig. S7. For P-SWCNT, LUMO and HOMO were uniformly delocalized throughout NT sidewall along C-C bonds, parallel and perpendicular to CNT axis, respectively. However, for f-CNTs with carboxyl and hydroxyl groups, the distribution of HOMO and LUMO orbitals on the surface of CNT was non-uniform (Fig. S7). It is noteworthy that orbitals at functionalized points had higher accumulation and strength than pristine CNTs. Fig. S7 presents the distributions of LUMO and HOMO of DOX molecules on its aromatic ring and on C or O atoms as well as C-C, C-O and O-H bonds. It was seen in Fig. 8 that, in the complexes with the highest stability (C and F), HOMO was distributed on DOX molecule and LUMO was localized on the surface of f-CNTs, indicating that electrons were transferred from DOX to f-CNTs. Hardness and energy gap values of NTs were lower than those of DOX. This meant that NTs were more polarizable than DOX and therefore, NTs could accept electrons from DOX molecules.

Table 6 presents the values of LUMO, HOMO and E_g for all studied models in both phases revealing the variations of E_g for P-CNT, f-CNT1 and f-CNT2 complexes in aqueous phase in the range of 4.038 eV, (4.268–4.285 eV) and (2.947-2.959), respectively. Low values of E_g meant low kinetic stability and high chemical reactivity for all of evaluated systems. Systems containing carboxylated CNTs had the lowest E_g values and the difference of E_g values in aqueous and gas phases for this system was higher than those of other complexes. Also, E_g had higher values in gas phase which indicated that in this phase, chemical reactivity was lower and kinetic stability was higher. It is also noteworthy that lower values of gap energy indicated semi-conductive behavior of structure. The data presented in Table 6 revealed slight variations of E_{LUMO} and E_{HOMO} for all complexes before and after adsorption which were almost the same as LUMO and HOMO energies of isolated NTs in two phases. Therefore, electrophilicity, energy gap, softness and hardness were not remarkably changed in various complexes indicating that upon the adsorption of DOX onto NTs, the electronic characteristics of the evaluated complexes were not changed significantly. As such, charge transfer between DOX and NTs molecules was insignificant. In drug delivery systems, this is an ideal interaction since drug molecules could be simply released from NT surface. Furthermore, the values of chemical potential NTs before and after DOX adsorption were negative, indicating that the investigated complexes were stable.

Table 6. Dipole moments (μ) (Debye), HOMO (E_{HOMO}) and LUMO (E_{LUMO}) energies, gap energy (E_g), quantum molecular descriptors, chemical hardness (η), chemical softness (S), chemical potential (μ), electronegativity (X), electrophilicity index (ω) (all in eV) calculated at WB97XD/6-31+G(d, p) level for DOX, SWCNT, f-SWCNT and different DOX molecules adsorbed by pristine and functionalized (6,6) armchair SWCNT

COMPLEX	Phase	(μ)	E_{HOMO}	E_{LUMO}	E_g	(η)	(S)	(μ)	(X)	(ω)
DOX	PCM	4.294	-6.911	-0.194	6.717	3.358	0.297	-3.552	3.552	1.879
	GAS	3.701	-6.857	-0.129	6.728	3.364	0.297	-3.493	3.493	1.815
SWCNT	PCM	0.000	-5.771	-1.733	4.038	2.019	0.495	-3.752	3.752	3.486
	GAS	0.000	-5.597	-1.552	4.045	2.022	0.494	-3.574	3.574	3.158
f-CNT1	PCM	12.749	-6.345	-2.050	4.295	2.147	0.465	-4.197	4.197	4.102
	GAS	6.024	-6.168	-1.859	4.309	2.154	0.464	-4.013	4.013	3.738
f-CNT2	PCM	32.688	-5.563	-2.480	3.083	1.541	0.649	-4.021	4.021	5.247
	GAS	2.711	-5.446	-2.027	3.419	1.709	0.585	-3.736	3.736	4.083
A	PCM	10.791	-5.701	-1.663	4.038	2.019	0.495	-3.682	3.682	3.357
	GAS	8.432	-5.436	-1.411	4.025	2.012	0.497	-3.423	3.423	2.911
B	PCM	9.041	-6.340	-2.055	4.285	2.142	0.466	-4.197	4.197	4.112
	GAS	5.447	-6.103	-1.807	4.296	2.148	0.465	-3.955	3.955	3.641
C	PCM	11.382	-6.372	-2.099	4.273	2.136	0.468	-4.235	4.235	4.199
	GAS	7.170	-6.234	-1.931	4.427	2.213	0.452	-4.082	4.082	3.764
D	PCM	14.223	-6.336	-2.068	4.268	2.134	0.468	-4.202	4.202	4.137
	GAS	8.350	-6.276	-2.001	4.275	2.137	0.468	-4.138	4.138	4.006
E	PCM	22.505	-5.425	-2.466	2.959	1.479	0.676	-3.945	3.945	5.261
	GAS	6.121	-5.512	-2.094	3.418	1.709	0.585	-3.803	3.803	6.532
F	PCM	22.474	-5.384	-2.433	2.951	1.475	0.678	-3.908	3.908	5.178
	GAS	3.689	-5.454	-2.020	3.434	1.717	0.582	-3.737	3.737	4.066

G	PCM	23.154	-5.410	-2.463	2.947	1.473	0.678	-3.936	3.936	5.260
	GAS	4.822	-5.354	-1.914	3.440	1.720	0.581	-3.634	3.634	3.839

More comprehensive evaluation of the electrophilicity index and chemical potential of the considered fragments confirmed that electron flow occurred spontaneously from DOX to NTs, because electrons being transferred from higher chemical potential. As an electrophilic species, NTs can accept electrons from drug molecules during adsorption process. Also, it was observed that the dipole moments of the evaluated configurations were improved by phase change from gas to aqueous. This difference was significant in f-CNT2 systems. Hardness ɳ values revealed that DOX molecules were harder than NTs and drug hardness was found to decrease by adsorption. In addition, this work confirmed that the addition of -OH and -COOH functional groups increased the polarity and therefore, the solubility of NTs.

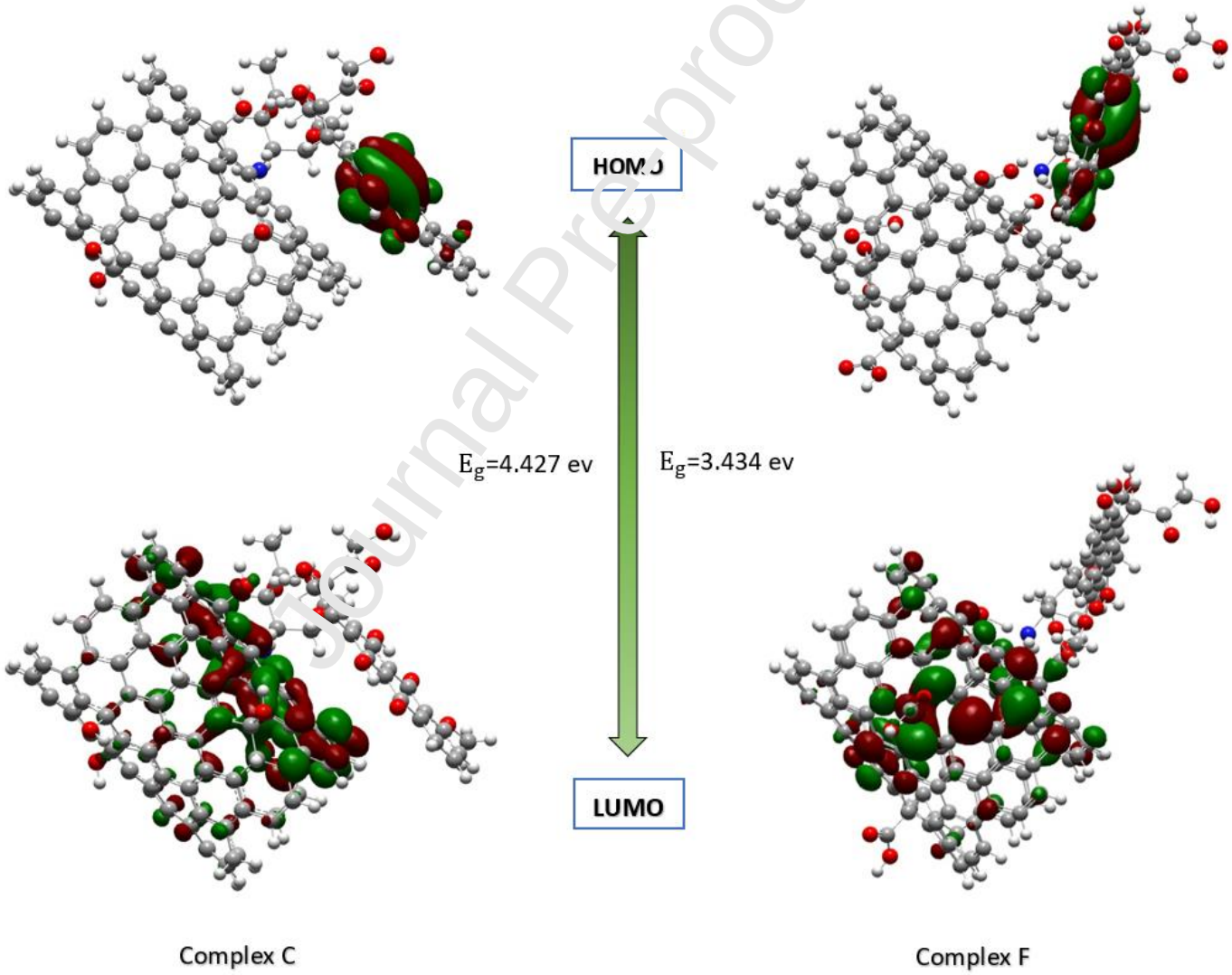

Fig. 8. Orbital diagrams of HOMO and LUMO in most stable complexes (C and F) in gas phase

The individual interaction of NTs and DOX molecules, including individual energy changes of acceptor ($\Delta E_{A(B)}$) and donor ($\Delta E_{B(A)}$), calculated and results are summarized in Table 7.

Table 7. The values of charge transfer (ΔN), individual energy change of acceptor ($\Delta E_{A(B)}$), individual energy change of donor ($\Delta E_{B(A)}$), and overall stabilization energy ($\Delta E_{SE(AB)}$), (all in eV) within reacting DOX drug molecule and NTs in aqueous and gas phases

Fragment	ΔN		$\Delta E_{A(B)}$		$\Delta E_{B(A)}$		$\Delta E_{SE(AB)}$	
	PCM	GAS	PCM	GAS	PCM	GAS	PCM	GAS
P-CNT	0.0371	0.0150	-0.1378	-0.0534	0.1341	0.0527	-0.0037	-0.0007
f-CNT1	0.1172	0.0942	-0.4771	-0.3684	0.4326	0.3439	-0.0445	-0.0245
f-CNT2	0.0957	0.0479	-0.3777	-0.1770	0.3553	0.1712	-0.0224	-0.0058

In this study, the kinetic properties of DOX-CNT interaction have been evaluated using $\Delta E_{B(A)}$, whereas $\Delta E_{A(B)}$ and $\Delta E_{SE(AB)}$ were employed to examine the thermodynamic stability of products. First, we assumed NT and DOX molecules and acceptor (A) and donor (B), respectively. ΔN values for DOX/NT complexes were positive which confirmed that electron flow direction was from DOX to NT. It is noteworthy that charge transfer rate in studied complexes in aqueous phase was higher than that in gas phase. Negative $\Delta E_{A(B)}$ value confirmed that the complex was more stable than isolated NT and DOX molecules. However, positive $\Delta E_{B(A)}$ value showed energetically promising process; in other words, electrons were transferred from DOX as donor to NT as acceptor. Finally, negative $\Delta E_{SE(AB)}$ value revealed the thermodynamic stability of the complexes.

Also, with further attention to chemical potential values given for DOX and CNT molecules in Table 6, it could be concluded that electron flow took place from drug molecule to nanotube. Also, electrophilicity and chemical potential values of the above components confirmed the mentioned electron flow direction. This electron flow along a single direction resulted in significant changes in the polarization of above complexes after adsorption. These results provided acceptable information on the intensity of interaction, stability, and toxicity of different chemical species such as the protonation of drug molecules in in media with different pH values which could be employed in designing nanocarriers and discovery of drugs and decrease and save laboratory test durations.

3.1.6 Density of States Analysis

System DOS defines state number per energy interval at each energy level that available for electrons. Higher DOS values at a certain energy level denote the availability of several states for occupation. Zero DOS shows that at that energy level, there are no states available for occupation. As can be seen in Table 6, and Fig. 9, comparison of E_g values showed that after DOX adsorption onto NTs, the energy gap of nanotube was not considerably changed. According to Fig. 9 the total density of states (TDOS) plots of complexes were almost similar to that of PDOS NTs. The only difference is that, comparison of peak heights at the highest energy level showed that DOS level in functionalized CNT systems were higher than those of system A which showed that CNTs had more states for

occupation. Also, unlike complex A, no hybridization occurred between CNT PDOS and TDOS which indicated more favorable physical adsorption in these systems.

It is noteworthy that energy gap was the energy range of a molecule in which no electron states existed. In DOS graphs, E_g is energy difference between conduction (LUMO) and valence (HOMO) levels. This corresponded to the energy required for outer shell electron release from its orbital around the nucleus to become a movable charge carrier capable of moving freely in material matrix. Therefore, E_g was a major factor in the determination of electrical conductivity in a material. Our results showed that the functionalization of pristine CNTs with carboxyl group decreased energy gap from 4.038 to 3.083 eV. Therefore, this type of functionalization shifted the behavior of CNT toward semiconductors while functionalization with hydroxyl increased energy gap by 0.257 eV and insulator properties of CNTs.

To study DOX adsorption effect on electronic structures of functionalized CNTs, PDOS and TDOS of P-CNT COMPLEX (complex A) and the most stable configurations (C and F) are shown in Fig. 9. PDOS plot mainly shows fragment orbital compositions contributing to molecular orbitals. PDOS results of the most stable complexes revealed that the main contribution to HOMO orbital came from DOX molecules (Fig. 9). On the other hand, the value of LUMO for CNTs was higher than that of DOX molecule; i.e., it participates in adsorption process through its LUMO orbital. As presented in Fig. 9, no considerable hybridization occurred during adsorption process between DOX and NT's orbitals. Also, comparison of curves showed that the possibility of this hybridization was decreased according to the following order *f*-CNT2 < *f*-CNT1 < P-CNT which confirmed the physical adsorption of drug molecule has enhanced on functional CNT's surface.

Fig. 9. The calculated total and projected electronic density of states (TDOS and PDOS) (a) complex A, (b) complex C, (c) complex F

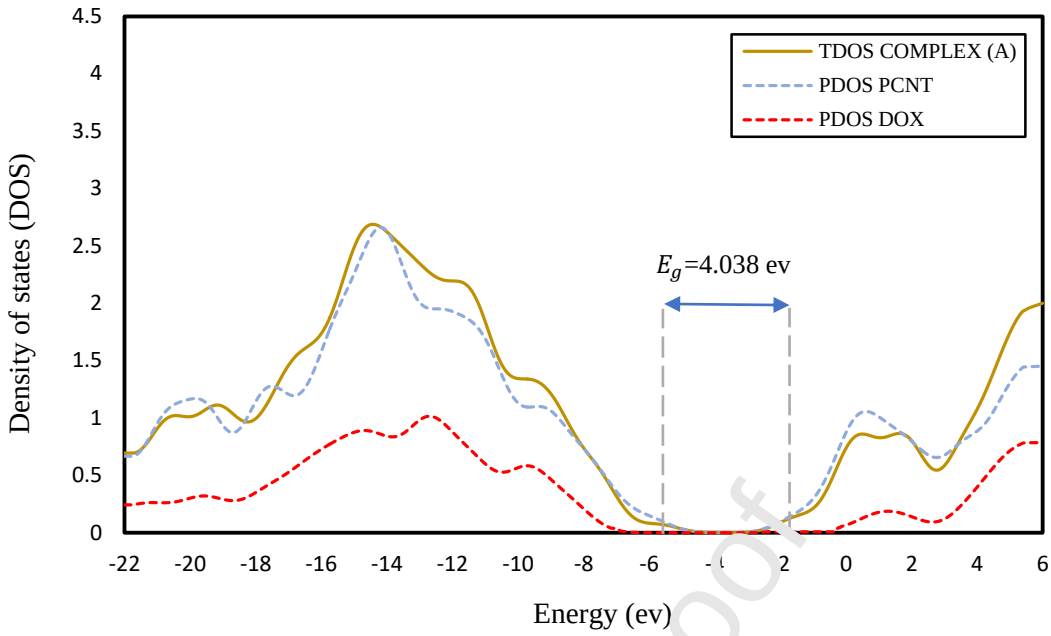

(a)

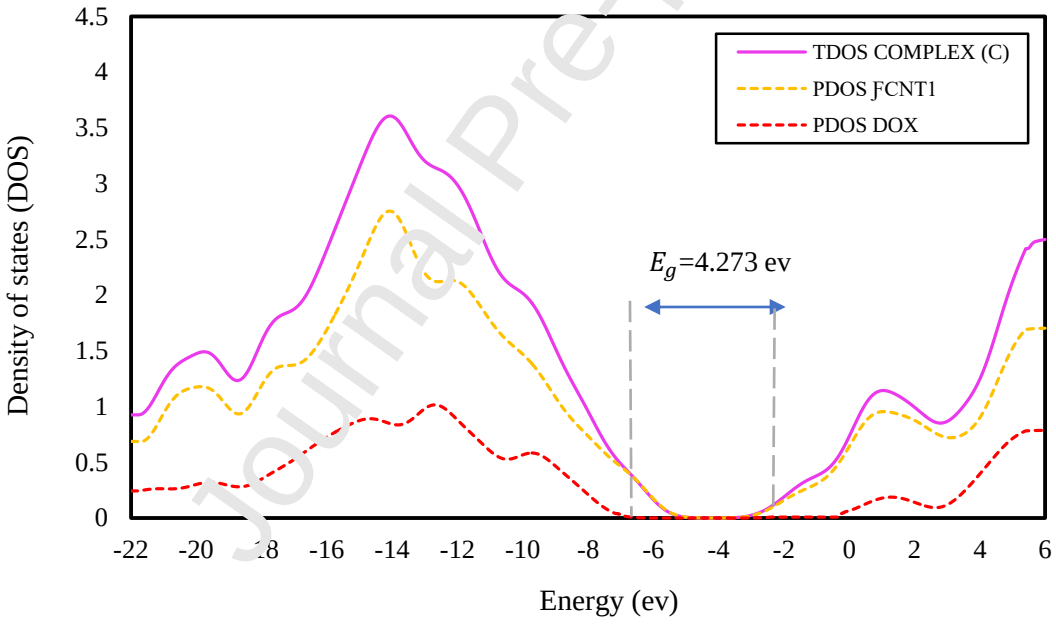

(b)

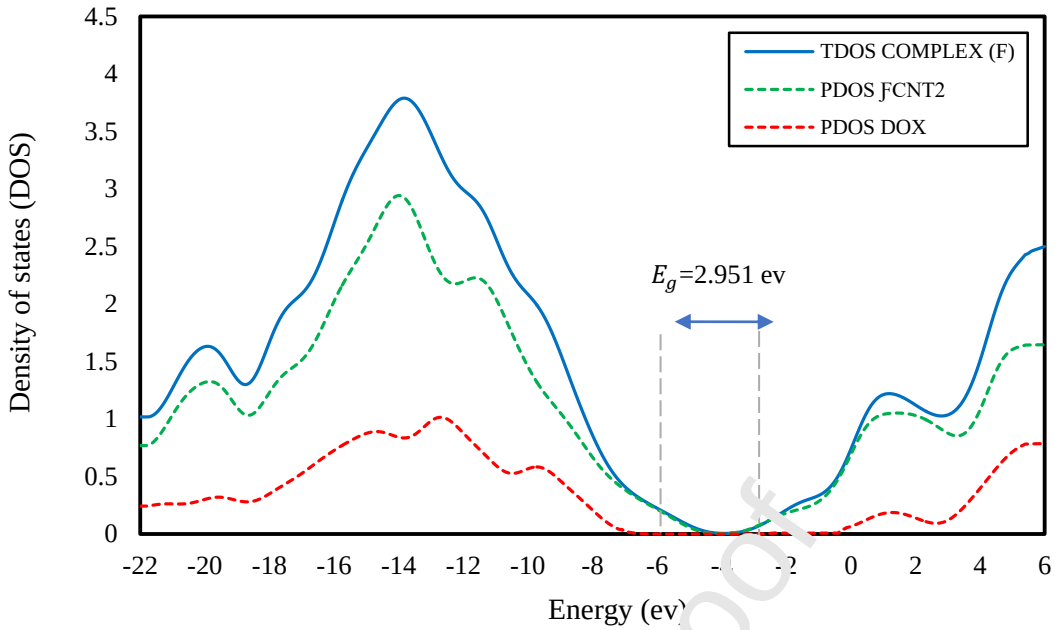

(c)

3.1.7 NBO Analysis

NBO analyses were also conducted to determine charge delocalization and orbital interactions at the same DFT theory level [86–88]. For better understanding intermolecular interactions in the evaluated complexes, NBO analyses were conducted which provided a great amount of information on the strength and nature of intermolecular interactions in terms of local orbital interactions and their second-order perturbation energy ($E^{(2)}$). Table 8 lists the results obtained from NBO analyses on all investigated complexes. These analyses also demonstrated significant charge transfer between DOX and functionalized CNT molecules in DOX/f-CNTs interaction unlike pristine CNT which was insignificant. NBO analyses showed that DOX tended to transfer of electrons to NTs during adsorption process. Therefore, in all of the evaluated complexes, drug molecules acted as donor and NTs acted as acceptor, and charge transfer occurred in DOX→ NTs direction. The calculated second-order perturbation interaction energy ($E^{(2)}$) for DOX/CNT, DOX/f1-CNT and DOX/f2-CNT systems were in the ranges of 0.12-2.95 and 0.06-42.34 and 0.05-69.37 Kcal/mol, respectively. The obtained results revealed that total charge transfer energies of functionalized CNT complexes were significantly higher than that of P-CNT complex and corresponding values for DOX/f2-CNT configurations were higher than those of DOX/f1-CNT complexes. It was witnessed that electron transfer was a key factor facilitating the adsorption of the molecules on the adsorbent. It was also found that higher energy values (E^2) for DOX adsorption onto CNT resulted in a greater extent of interaction between DOX and CNT molecules.

The theoretical findings of this work illustrated that in hydroxylated CNT systems at configurations B, lone electron pair of O216 in drug molecule acted as donor through H158 atom on O-H group of the functionalized CNT, and f1-CNT acted as acceptor in intermolecular charge transfer interactions at energy levels of 13.01 and 14.64 Kcal/mol in gas and aqueous phases, respectively. In complex C, lone pairs of atoms O159, O214 and N224 in DOX acted as donor through H203, H166 and H158 atoms of f-CNT1 as an acceptor respectively. The $E^{(2)}$ values of these pairs are summarized in Table 8 for aqueous and gas phases. The strongest intermolecular interaction was observed for configuration C which, compared to other complexes in hydroxylated CNT systems, had the highest total charge transfer energies of 36.43 for and 42.34 Kcal/mol for O-H and N-H in gas and aqueous phases, respectively. In complex D, the lone pair of O191 atom in DOX acts as a donor with lone pair H163 atom of f1-CNT as acceptor with energy values of 16.81 and 10.34 Kcal/mol in aqueous and gas phases, respectively.

The data provided in Table 8 showed that the highest $E^{(2)}$ energies were obtained for complexes E, F and G in systems with carboxylated CNTs. In complex E, a lone bond was formed between atom O226 of drug molecule as donor and H176 of carboxyl on CNT as acceptor with $E^{(2)}$energies of 50.16 and 50.41 Kcal/mol in aqueous and gas phases, respectively. In system F, two dominant lone bonds occurred between N234 of drug as electron donor and H176 of CNT as electron acceptor as well as O203 of drug and H175 of CNT with $E^{(2)}$energies of 69.3 and 66.46 Kcal/mol as well as 23.83 and 21.78 Kcal/mol in aqueous and gas phases, respectively. The obtained results showed that system F had the highest stability which confirmed the results obtained in the previous section. In complex G, three dominant bonds were formed between O-H----H and H----O in drug and f2-CNT molecules two of which, i.e. those between O224 and O201 as well as H176 and H175 with energy values of 55.29 and 20.51 Kcal/mol in aqueous phases, respectively, drug molecule acted as electron donor and CNT acted as electro n acceptor while in the other bond between O168 of carbonyl group on CNT acted as electron donor and H218 of drug acted as electron acceptor which had $E^{(2)}$ energy levels of 13.29 and 13.85 Kcal/mol in aqueous and gas phases, respectively. According to $E^{(2)}$ energy levels in this model, it was concluded that generally drug molecules acted as electron donor and CNT acted as acceptor.

Table 8. The second-order perturbation energy ($E^{(2)}$), Kcal/mol, corresponds to the charge flow between the NT's and DOX molecule in the PCM and gas phase

Model	Donor	Acceptor	$E^{(2)}$ (Kcal/mol)	
			PCM	GAS
A	LP (1) O 151	σ*(1) C 61 - H 104	2.95	---
	LP (1) O 151	σ*(1) C 49 - H 102	---	2.53
	LP (3) O 155	σ*(1) H 107	0.12	---

B	LP (1) O 216	LP*(1) H 158	14.64	13.01
	σ *(1) C 2-C 11	π*(1) H 223	0.35	0.31
	σ *(1) C 10-C 24	π*(1) H 199	0.25	0.27
C	LP (2) O 159	LP*(1) H 203	36.43	21.49
	LP (2) O 214	LP*(1) H 166	23.71	---
	LP (1) N 224	LP*(1) H 158	---	42.34
	LP (3) O 157	π*(1) H 225	0.21	---
	LP (1) O 157	σ*(1) N 224 - H 225	1.40	---
	σ (1) C 21 - C 22	π*(1) H 236	0.06	---
	σ (1) C 10 - C 24	π*(1) H 228	0.11	---
D	LP (1) O 191	LP*(1) H 163	16.81	10.34
	LP (2) O 159	LP*(1) H 203	---	21.49
	LP (3) O 160	π*(1) H 189	0.50	0.27
	LP (3) O 159	π*(1) H 205	0.15	0.14
	σ (1) C 39 - C 41	π*(1) H 205	---	0.13
E	LP (2) O 226	LP*(1) H 176	50.16	50.41
	LP (1) O 171	σ*(1) C 208 - H 209	1.15	2.16
	LP (3) O 170	π*(1) H 233	0.12	0.17
	LP (1) O 168	σ*(1) N 234 - H 235	2.46	2.56
	LP (1) O 201	σ*(1) C 128 - H 138	0.21	---
F	LP (1) O 203	LP*(1) H 175	23.83	21.78
	LP*(1) H 175	π*(1) O 126	0.05	---
	LP*(1) H 205	π*(1) O 168	0.06	---
	LP (1) N 234	LP*(1) H 176	69.37	66.46
	σ (1) C 23 - C 24	π*(1) H 236	0.18	---
G	LP (2) O 224	σ*(1) O 170 - H 176	---	36.97
	LP (2) O 224	LP*(1) H 176	55.29	---
	LP (1) O 201	σ*(1) O 167 - H 175	---	18.53
	LP (1) O 201	LP*(1) H 175	20.51	---
	LP (1) O 168	LP*(1) H 218	13.29	13.85

3.1.8 Molecular Electrostatic Potential (MEP)

Molecular electrostatic potential (MEP) at a certain point near a molecule indicates net electrostatic effect generated at that point through total distribution of charge in the molecule. MEP is an important factor when studying reactivity describing that an approaching electrophile would be attracted to negative sites (in which the effect of electron distribution is dominant). The significance of MEP is because it gives the shape and size of the molecule and determines its negative, neutral and positive electrostatic potential regions as color grading and provides a powerful tool in investigating the relationship between molecular structure and its physiochemical characteristics [89,90]. Different electrostatic potential values at surface were shown in different colors such that red shows the most negative electrostatic potential, green shows zero potential regions, blue shows the most positive electrostatic potential. Potential was increased in the order of red<orange<yellow<green<blue. According to MEP plots presented in Fig. 10, O atoms were red (negatively charged) and N and H atoms were intensively blue (positively charged). This meant that the most intensive electron transfer occurred from electropositive atoms (N and H) to the electronegative one (O). However, as can be

seen in the most stable complexes (C and F) Due to their electropositive property, N and H atoms in DOX tended to bond to electronegative O and less electropositive H atoms in functionalized CNT molecules.

Fig. 10. Molecular electrostatic potential (MEP) surfaces of (a) DOX (b) P-CNT (c) *f*-CNT1 (d) *f*-CNT2 (e) complex A (f) complex C and (g) complex F obtained at WB97XD/6-31+G (d, p) level

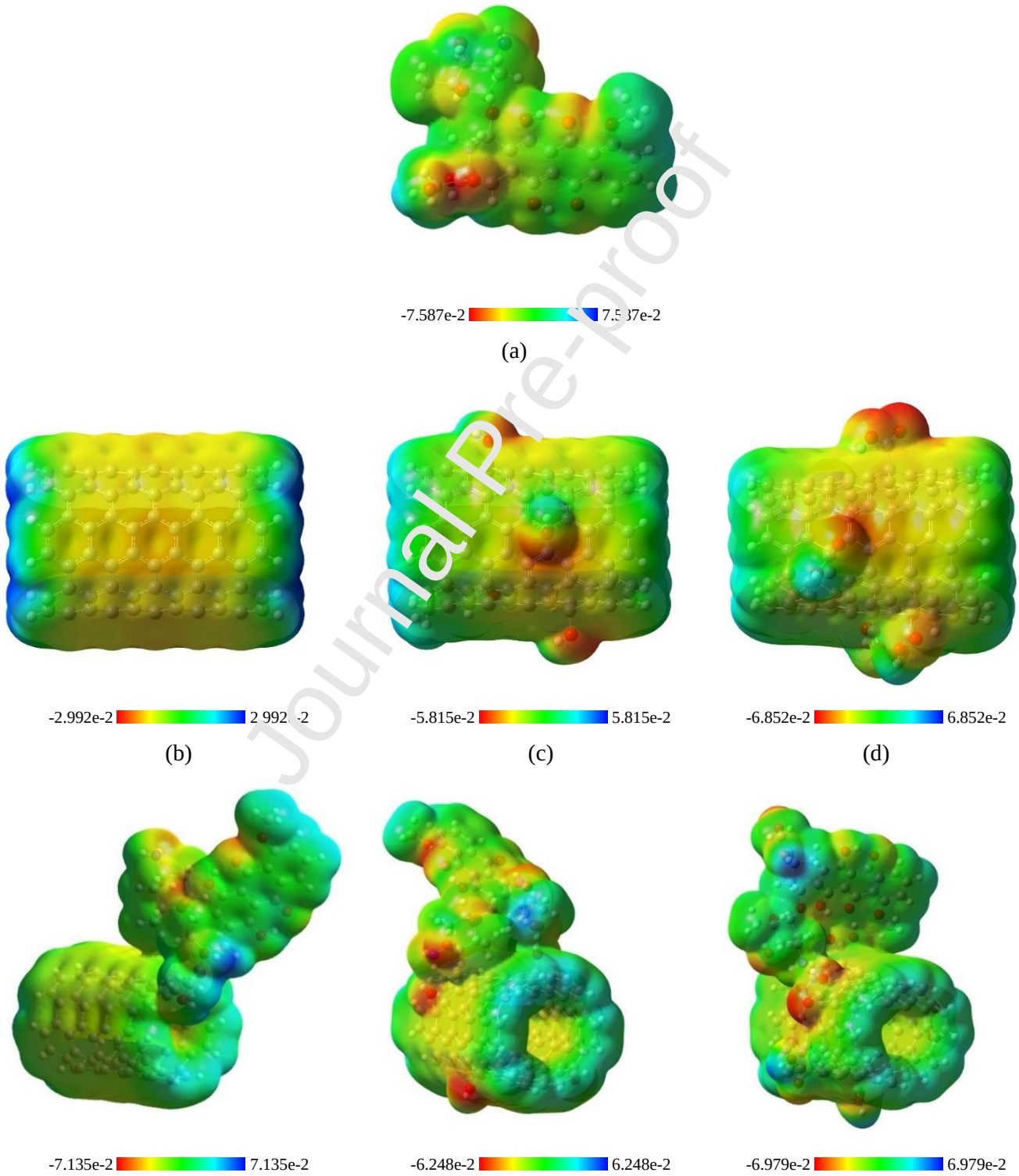

(e) (f) (g)

4. Conclusion

In this work, for the first time as a comprehensive research, the nature of interactions between active points of anticancer drug DOX and outer surfaces of pristine and -COOH and -OH functionalized CNTs in aqueous and gas phases have been investigated using DFT calculations. Geometrical analyses showed that bond distance between the atoms of drug molecule before and after being adsorbed onto the outer surface of CNT was not significantly changed which indicated its stability. Negative values of adsorption energy in the investigated complexes in aqueous and gas phases showed that the interactions between DOX and CNT molecules were favorable and the process was physisorption and exothermal. Also, the values of these energies showed that the functionalization of CNT, especially with –COOH functional group, improved the adsorption of drug molecule onto CNT and therefore, intermolecular hydrogen bonds have important role in the stability of physisorption. The results also showed that adsorption process was more stable and favorable in gas phase. QTAIM calculations showed that the nature of bonds was electrostatic and partially covalent and there was a direct relation between the distance and strength of bond which was even stronger in systems with functionalized CNTs. Also, the electronic properties and descriptors of the considered systems were calculated in aqueous and gas phases and the obtained results showed that the functionalization of CNTs with –COOH and –OH groups gave them semiconductor and metallic properties, respectively. The values of electrophilicity and chemical potential showed that electron flow occurred from drug molecule to nanotube. Negative enthalpy and Gibbs free energy values in the studied systems indicated that adsorption process was exothermic and thermodynamically favorable. Also, NBO calculations showed that adsorption was achieved through electron transfer from drug molecule to CNT. In the other side, the value of perturbation energy in systems containing COOH-functionalized CNTs was higher than those containing OH-functionalized CNTs and those of both were higher than that of systems with pristine CNTs. Also, DOS results showed that, unlike pristine CNTs, there was not adequate hybridization between drug and CNT molecules in functionalized systems, which indicated stable adsorption process.

Acknowledgement

Prof. Jen and Mr. Karimzadeh would like to acknowledge the financial support from Global Excellence Statue (GES) Fellowship and National Research Foundation (NRF) of South Africa. Also, the computation platforms were provided by Center of High Performance Computing (CHPC) at Cape Town and University of Johannesburg IT service is also gracefully acknowledged.

Author Statement

Mr. Sina Karimzadeh: Conceptualization, Methodology, Validation, Investigation, Writing - Original Draft, Visualization.

Prof Babak Safaei; Methodology, Software, Data Curation, Formal analysis.

Professor Tien-Chien Jen: Project administration, Conceptualization, Validation, Resources, Writing - Review & Editing, Visualization, Supervision, Funding.

Declaration of interests

☒ The authors declare that they have no known competing financial interests or personal relationships that could have appeared to influence the work reported in this paper.

References

[1] S. Xie, W. Li, Z. Pan, B. Chang, S. Lianfeng, Mechanical and physical properties on carbon nanotube, J. Phys. Chem. Solids. 61 (2000) 1153–1158. https://doi.org/10.1016/S0022-3697(99)00376-5.

[2] B. Safaei, P. Naseradinmousavi, A. Rahmani, Development of an accurate molecular mechanics model for buckling behavior of multi-walled carbon nanotubes under axial compression, J. Mol. Graph. Model. 65 (2016) 43–60. https://doi.org/10.1016/j.jmgm.2016.02.001.

[3] C. Velasco-Santos, A.L. Martínez-Hernández, F.T. Fisher, R. Ruoff, V.M. Castaño, Improvement of Thermal and Mechanical Properties of Carbon Nanotube Composites through Chemical Functionalization, Chem. Mater. 15 (2003) 4470–4475. https://doi.org/10.1021/cm034243c.

[4] W. Zhang, Z. Zhang, Y. Zhang, The application of carbon nanotubes in target drug delivery systems for cancer therapies, Nanoscale Res. Lett. 6 (2011) 555. https://doi.org/10.1186/1556-276X-6-555.

[5] S.K. Vashist, D. Zheng, G. Pastorin, K. Al-Rubeaan, J.H.T. Luong, F.S. Sheu, Delivery of drugs and biomolecules using carbon nanotubes, Carbon N. Y. 49 (2011) 4077–4097. https://doi.org/10.1016/j.carbon.2011.05.049.

[6] E. Heister, E.W. Brunner, G.R. Dieckmann, I. Jurewicz, A.B. Dalton, Are carbon nanotubes a natural solution? applications in biology and medicine, ACS Appl. Mater. Interfaces. 5 (2013) 1870–1891. https://doi.org/10.1021/am302902d.

[7] V. Raffa, G. Ciofani, O. Vittorio, C. Riggio, A. Cuschieri, Physicochemical properties affecting cellular uptake of carbon nanotubes, Nanomedicine. 5 (2010) 89–97. https://doi.org/10.2217/nnm.09.95.

[8] P. Liu, Modification strategies for carbon nanotubes as a drug delivery system, Ind. Eng. Chem. Res. 52 (2013) 13517–13527. https://doi.org/10.1021/ie402360f.

[9] A.C. Tripathi, S.A. Saraf, S.K. Saraf, Carbon nanotropes: A contemporary paradigm in drug delivery, Materials (Basel). 8 (2015) 3068–3100. https://doi.org/10.3390/ma8063068.

[10] H. Zhao, R. Ding, X. Zhao, Y. Li, L. Qu, H. Pei, L. Yildirimer, Z. Wu, W. Zhang, Graphene-based nanomaterials for drug and/or gene delivery, bioimaging, and tissue engineering, Drug Discov. Today. 22 (2017) 1302–1317. https://doi.org/10.1016/j.drudis.2017.04.002.

[11] F. Chekin, V. Myshin, R. Ye, S. Melinte, S.K. Singh, S. Kurungot, R. Boukherroub, S. Szunerits, Graphene-modified electrodes for sensing doxorubicin hydrochloride in human plasma, Anal. Bioanal. Chem. 411 (2019) 1509–1516. https://doi.org/10.1007/s00216-019-01611-w.

[12] S. Augustine, J. Singh, M. Srivastava, M. Sharma, A. Das, B.D. Malhotra, Recent advances in

carbon based nanosystems for cancer theranostics, Biomater. Sci. 5 (2017) 901–952. https://doi.org/10.1039/c7bm00008a.

[13] T. Nozaki, K. Ohnishi, K. Okazaki, U. Kortshagen, Fabrication of vertically aligned single-walled carbon nanotubes in atmospheric pressure non-thermal plasma CVD, Carbon N. Y. 45 (2007) 364–374. https://doi.org/10.1016/j.carbon.2006.09.009.

[14] K.A. Worsley, I. Kalinina, E. Bekyarova, R.C. Haddon, Functionalization and dissolution of nitric acid treated single-walled carbon nanotubes, J. Am. Chem. Soc. 131 (2009) 18153–18158. https://doi.org/10.1021/ja906267g.

[15] E.C. Dandley, A.J. Taylor, K.S. Duke, M.D. Ihrie, K.A. Shipkowski, G.N. Parsons, J.C. Bonner, Atomic layer deposition coating of carbon nanotubes with zinc oxide causes acute phase immune responses in human monocytes in vitro and in mice after pulmonary exposure, Part. Fibre Toxicol. 13 (2015) 29. https://doi.org/10.1186/s12989-016-0141-9.

[16] S. Vardharajula, S.Z. Ali, P.M. Tiwari, E. Eroğlu, K. Vig, V.A. Dennis, S.R. Singh, Functionalized carbon nanotubes: Biomedical applications, Int. J. Nanomedicine. 7 (2012) 5361–5374. https://doi.org/10.2147/IJN.S35832.

[17] S. Yuan, L. Zeng, Y. Zhuang, Q. Hou, M. Song, Functionalized single-walled carbon nanotubes for the improved solubilization and delivery of curcumin, Fullerenes Nanotub. Carbon Nanostructures. 24 (2016) 13–19. https://doi.org/10.1080/1536383X.2015.1088007.

[18] T. Kuretake, S. Kawahara, M. Motooka, S. Uno, An Electrochemical Gas Biosensor Based on Enzymes Immobilized on Chromatography Paper for Ethanol Vapor Detection, Sensors. 17 (2017) 281. https://doi.org/10.3390/s17020281.

[19] Y. Zhu, X. Liu, K.W.K. Yeung, P.K. Chu, S. Wu, Biofunctionalization of carbon nanotubes/chitosan hybrids on Ti implants by atomic layer deposited ZnO nanostructures, Appl. Surf. Sci. 400 (2017) 14–23. https://doi.org/10.1016/j.apsusc.2016.12.158.

[20] S. Niyogi, M.A. Hamon, H. Hu, B. Zhao, P. Bhowmik, R. Sen, M.E. Itkis, R.C. Haddon, Chemistry of single-walled carbon nanotubes, Acc. Chem. Res. 35 (2002) 1105–1113. https://doi.org/10.1021/ar010155r.

[21] B. Kuhn, P. Mohr, M. Stahl, Intramolecular hydrogen bonding in medicinal chemistry, J. Med. Chem. 53 (2010) 2601–2611. https://doi.org/10.1021/jm100087s.

[22] K.M. Hutchins, Functional materials based on molecules with hydrogen-bonding ability: Applications to drug co-crystals and polymer complexes, R. Soc. Open Sci. 5 (2018). https://doi.org/10.1098/rsos.180564.

[23] M. Yoosefian, A. Pakpour, N. Etminan, Nanofilter platform based on functionalized carbon nanotubes for adsorption and elimination of Acrolein, a toxicant in cigarette smoke, Appl. Surf. Sci. 444 (2018) 598–603. https://doi.org/10.1016/j.apsusc.2018.03.108.

[24] M. Yoosefian, A. Pakpour, M. Zahedi, Carboxylated single-walled carbon nanotubes as a semiconductor for adsorption of acrylamide in mainstream cigarette smoke, Phys. E Low-Dimensional Syst. Nanostructures. 124 (2020) 114299. https://doi.org/10.1016/j.physe.2020.114299.

[25] X. Zhang, L. Meng, Q. Lu, Z. Fei, P.J. Dyson, Targeted delivery and controlled release of doxorubicin to cancer cells using modified single wall carbon nanotubes, Biomaterials. 30 (2009) 6041–6047. https://doi.org/10.1016/j.biomaterials.2009.07.025.

[26] O. Tacar, P. Sriamornsak, C.R. Dass, Doxorubicin: An update on anticancer molecular action, toxicity and novel drug delivery systems, J. Pharm. Pharmacol. 65 (2013) 157–170. https://doi.org/10.1111/j.2042-7158.2012.01567.x.

[27] M. Baxter-Holland, C.R. Dass, Doxorubicin, mesenchymal stem cell toxicity and antitumour activity: implications for clinical use, J. Pharm. Pharmacol. 70 (2018) 320–327. https://doi.org/10.1111/jphp.12869.

[28] D.P. Cormode, T. Skajaa, Z.A. Fayad, W.J.M. Mulder, Nanotechnology in medical imaging: Probe design and applications, Arterioscler. Thromb. Vasc. Biol. 29 (2009) 992–1000. https://doi.org/10.1161/ATVBAHA.108.165506.

[29] Z. Liu, A.C. Fan, K. Rakhra, S. Sherlock, A. Goodwin, X. Chen, Q. Yang, D.W. Felsher, H.

Dai, Supramolecular stacking of doxorubicin on carbon nanotubes for in vivo cancer therapy, Angew. Chemie - Int. Ed. 48 (2009) 7668–7672. https://doi.org/10.1002/anie.200902612.

[30] H. Sharma, K. Kumar, C. Choudhary, P.K. Mishra, B. Vaidya, Development and characterization of metal oxide nanoparticles for the delivery of anticancer drug, Artif. Cells, Nanomedicine, Biotechnol. 44 (2016) 672–679. https://doi.org/10.3109/21691401.2014.978980.

[31] T.M. Allen, P.R. Cullis, Liposomal drug delivery systems: From concept to clinical applications, Adv. Drug Deliv. Rev. 65 (2013) 36–48. https://doi.org/10.1016/j.addr.2012.09.037.

[32] A. Almeida, M. Araújo, R. Novoa-Carballal, F. Andrade, H. Gonçalves, R.L. Reis, M. Lúcio, S. Schwartz, B. Sarmento, Novel amphiphilic chitosan micelles as carriers for hydrophobic anticancer drugs, Mater. Sci. Eng. C. 112 (2020) 110920. https://doi.org/10.1016/j.msec.2020.110920.

[33] A. Ali, S. Ahmed, A review on chitosan and its nanocomposites in drug delivery, Int. J. Biol. Macromol. 109 (2018) 273–286. https://doi.org/10.1016/j.ijbiomac.2017.12.078.

[34] Z. Xiao, L.B. Kong, S. Ruan, X. Li, S. Yu, X. Li, Y. Jiang, Z. Yao, S. Ye, C. Wang, T. Zhang, K. Zhou, S. Li, Recent development in nanocarbon materials for gas sensor applications, Sensors Actuators, B Chem. 274 (2018) 235–267. https://doi.org/10.1016/j.snb.2018.07.040.

[35] T.C. Lin, B.R. Huang, Palladium nanoparticles modified carbon nanotube/nickel composite rods (Pd/CNT/Ni) for hydrogen sensing, Sensors Actuators, B Chem. 162 (2012) 108–113. https://doi.org/10.1016/j.snb.2011.12.044.

[36] M. Yoosefian, N. Etminan, A. Juan, E. Mirhaji, Ultra-low concentration protein detection based on phenylalanine-Pd/SWCNT as a high sensitivity nanoreceptor, RSC Adv. 10 (2020) 2650–2660. https://doi.org/10.1039/c9ra09243a.

[37] Y. Sun, Z. Peng, H. Li, Z. Wang, Y. Mu, G. Zhang, S. Chen, S. Liu, G. Wang, C. Liu, L. Sun, B. Man, C. Yang, Suspended CNT-Based FET sensor for ultrasensitive and label-free detection of DNA hybridization, Biosens. Bioelectron. 137 (2019) 255–262. https://doi.org/10.1016/j.bios.2019.04.054.

[38] M. Cao, D. Wu, M. Yoosefian, S. Sabaei, M. Jahani, Comprehensive study of the encapsulation of Lomustine anticancer drug into single walled carbon nanotubes (SWCNTs): Solvent effects, molecular conformations, electronic properties and intramolecular hydrogen bond strength, J. Mol. Liq. 320 (2020) 114285. https://doi.org/10.1016/j.molliq.2020.114285.

[39] M. Yoosefian, S. Sabaei, N. Etminan, Encapsulation efficiency of single-walled carbon nanotube for Ifosfamide anti-cancer drug, Comput. Biol. Med. 114 (2019) 103433. https://doi.org/10.1016/j.compbiomed.2019.103433.

[40] M. Yoosefian, M. Jahani, A molecular study on drug delivery system based on carbon nanotube for the novel norepinephrine prodrug, Droxidopa, J. Mol. Liq. 284 (2019) 258–264. https://doi.org/10.1016/j.molliq.2019.04.016.

[41] L. Piela, Ideas of Quantum Chemistry: Second Edition, Elsevier B.V., 2013. https://doi.org/10.1016/C2011-0-05128-1.

[42] B. Mennucci, Polarizable continuum model, Wiley Interdiscip. Rev. Comput. Mol. Sci. 2 (2012) 386–404. https://doi.org/10.1002/wcms.1086.

[43] S. Miertuš, E. Scrocco, J. Tomasi, Electrostatic interaction of a solute with a continuum. A direct utilizaion of AB initio molecular potentials for the prevision of solvent effects, Chem. Phys. 55 (1981) 117–129. https://doi.org/10.1016/0301-0104(81)85090-2.

[44] M. Yoosefian, Powerful greenhouse gas nitrous oxide adsorption onto intrinsic and Pd doped Single walled carbon nanotube, Appl. Surf. Sci. 392 (2017) 225–230. https://doi.org/10.1016/j.apsusc.2016.09.051.

[45] A.B. Porto, L.F.C. de Oliveira, H.F. Dos Santos, Exploring the potential energy surface for reaction of SWCNT with NO2+: A model reaction for oxidation of carbon nanotube in acid solution, Comput. Theor. Chem. 1088 (2016) 1–8. https://doi.org/10.1016/j.comptc.2016.05.002.

[46] Z. Chen, Y. Li, Z. He, Y. Xu, W. Yu, Theoretical investigations on charge transport properties of tetrabenzo[*a,d,j,m*]coronene derivatives using different density functional theory functionals (B3LYP, M06-2X, and wB97XD), J. Chem. Res. 43 (2019) 293–303. https://doi.org/10.1177/1747519819861626.
[47] V. M. Frisch, G. Trucks, H. Schlegel, G. Scuseria, M. Robb, J. Cheeseman, G. Scalmani, G.P. Barone, B. Mennucci, Gaussian Inc., Wallingford CT, 2010., (n.d.).
[48] S.F. Boys, F. Bernardi, The calculation of small molecular interactions by the differences of separate total energies. Some procedures with reduced errors, Mol. Phys. 19 (1970) 553–566. https://doi.org/10.1080/00268977000101561.
[49] Atoms in Molecules - Richard F. W. Bader - Oxford University Press, (n.d.).
[50] R.F.W. Bader, P.M. Beddall, Virial field relationship for molecular charge distributions and the spatial partitioning of molecular properties, J. Chem. Phys. 56 (1972) 3320–3329. https://doi.org/10.1063/1.1677699.
[51] E. Nemati-Kande, R. Karimian, V. Goodarzi, E. Ghazizadeh, Feasibility of pristine, Al-doped and Ga-doped Boron Nitride nanotubes for detecting SF4 gas: A DFT, NBO and QTAIM investigation, Appl. Surf. Sci. 510 (2020) 145490. https://doi.org/10.1016/j.apsusc.2020.145490.
[52] F. Biegler-König, Calculation of Atomic Integration Data, J. Comput. Chem. 21 (2000) 1040–1048. https://doi.org/10.1002/1096-987X(200009)21:12<1040::AID-JCC2>3.0.CO;2-8.
[53] K.B. Wiberg, Application of the pople-santry-segal CNDO method to the cyclopropylcarbinyl and cyclobutyl cation and to bicyclobutane, Tetrahedron. 24 (1968) 1083–1096. https://doi.org/10.1016/0040-4020(68)88057-3.
[54] L.K. Harper, A.L. Shoaf, C.A. Bayse, Predicting Trigger Bonds in Explosive Materials through Wiberg Bond Index Analysis, ChemPhysChem. 16 (2015) 3886–3892. https://doi.org/10.1002/cphc.201500773.
[55] E. Espinosa, M. Souhassou, H. Lachekar, C. Lecomte, Topological analysis of the electron density in hydrogen bonds, Acta Crystallogr. Sect. B Struct. Sci. 55 (1999) 563–572. https://doi.org/10.1107/S0108768199002128.
[56] E. Espinosa, E. Molins, C. Lecomte, Hydrogen bond strengths revealed by topological analyses of experimentally observed electron densities, Chem. Phys. Lett. 285 (1998) 170–173. https://doi.org/10.1016/S0009-2614(98)00036-0.
[57] M. Lotfi, A. Morsali, M.R. Bozorgmehr, Comprehensive quantum chemical insight into the mechanistic understanding of the surface functionalization of carbon nanotube as a nanocarrier with cladribine anticancer drug, Appl. Surf. Sci. 462 (2018) 720–729. https://doi.org/10.1016/j.apsusc.2018.08.151.
[58] Y.A. Abramov, On the Possibility of Kinetic Energy Density Evaluation from the Experimental Electron-Density Distribution, Acta Crystallogr. Sect. A Found. Crystallogr. 53 (1997) 264–272. https://doi.org/10.1107/S010876739601495X.
[59] N. Bazhin, Useful Work and Gibbs Energy, in: Thermodyn. - Fundam. Its Appl. Sci., InTech, Croatia, 2012. https://doi.org/10.5772/50119.
[60] M.K. Hazrati, Z. Bagheri, A. Bodaghi, Application of C30B15N15 heterofullerene in the isoniazid drug delivery: DFT studies, Phys. E Low-Dimensional Syst. Nanostructures. 89 (2017) 72–76. https://doi.org/10.1016/j.physe.2017.02.009.
[61] W.B. Jensen, Electronegativity from Avogadro to Pauling: Part 1: Origins of the Electronegativity Concept, J. Chem. Educ. 73 (1996) 11. https://doi.org/10.1021/ed073p11.
[62] R.G. Parr, R.G. Pearson, Absolute Hardness: Companion Parameter to Absolute Electronegativity, J. Am. Chem. Soc. 105 (1983) 7512–7516. https://doi.org/10.1021/ja00364a005.
[63] R.G. Parr, L. V. Szentpály, S. Liu, Electrophilicity index, J. Am. Chem. Soc. 121 (1999) 1922–1924. https://doi.org/10.1021/ja983494x.
[64] A. Sarmah, S. Saha, P. Bagaria, R.K. Roy, On the complementarity of comprehensive decomposition analysis of stabilization energy (CDASE) - Scheme and supermolecular

approach, Chem. Phys. 394 (2012) 29–35. https://doi.org/10.1016/j.chemphys.2011.12.010.
[65] P. Bagaria, S. Saha, S. Murru, V. Kavala, B.K. Patel, R.K. Roy, A comprehensive decomposition analysis of stabilization energy (CDASE) and its application in locating the rate-determining step of multi-step reactions, Phys. Chem. Chem. Phys. 11 (2009) 8306–8315. https://doi.org/10.1039/b902335f.
[66] S. Saha, R.K. Roy, S. Pal, CDASE - A reliable scheme to explain the reactivity sequence between Diels-Alder pairs, Phys. Chem. Chem. Phys. 12 (2010) 9328–9338. https://doi.org/10.1039/b925441b.
[67] J. Wang, J. Liu, B. Zhang, X. Ji, K. Xu, C. Chen, L. Miao, J. Jiang, The mechanism of hydrogen adsorption on transition metal dichalcogenides as hydrogen evolution reaction catalyst, Phys. Chem. Chem. Phys. 19 (2017) 10125–10132. https://doi.org/10.1039/c7cp00636e.
[68] H.H. Huang, X. Fan, D.J. Singh, H. Chen, Q. Jiang, W.T. Zheng, Controlling phase transition for single-layer MTe2 (M = Mo and W): Modulation of the potential barrier under strain, Phys. Chem. Chem. Phys. 18 (2016) 4086–4094. https://doi.org/10.1039/c5cp06706e.
[69] H. Zhong, R. Quhe, Y. Wang, Z. Ni, M. Ye, Z. Song, Y. Pan, J. Yang, L. Yang, M. Lei, J. Shi, J. Lu, Interfacial Properties of Monolayer and Bilayer MoS 2 Contacts with Metals: Beyond the Energy Band Calculations, Sci. Rep. 6 (2016) 1–16. https://doi.org/10.1038/srep21786.
[70] C. Clay Marston, G.G. Balint-Kurti, The Fourier grid Hamiltonian method for bound state eigenvalues and eigenfunctions, J. Chem. Phys. 91 (1989) 3571–3576. https://doi.org/10.1063/1.456888.
[71] T. Lu, F. Chen, Multiwfn: A multifunctional wavefunction analyzer, J. Comput. Chem. 33 (2012) 580–592. https://doi.org/10.1002/jcc.22885.
[72] P. Wolski, K. Nieszporek, T. Panczyk, Carbon Nanotubes and Short Cytosine-Rich Telomeric DNA Oligomeres as Platforms for Controlled Release of Doxorubicin—A Molecular Dynamics Study, Int. J. Mol. Sci. 21 (2020) 3619. https://doi.org/10.3390/ijms21103619.
[73] Y. Wang, Z. Xu, Interaction mechanism of doxorubicin and SWCNT: Protonation and diameter effects on drug loading and releasing, RSC Adv. 6 (2015) 314–322. https://doi.org/10.1039/c5ra20866a.
[74] A. Rodríguez-Galván, O. Amelines Sarria, M. Rivera, M.D.P. Carreón-Castro, V.A. Basiuk, Adsorption and Self-Assembly of Anticancer Antibiotic Doxorubicin on Single-Walled Carbon Nanotubes, Nano. 11 (2016). https://doi.org/10.1142/S1793292016500387.
[75] S.N. Steinmann, P. Sautet, C. Michel, Solvation free energies for periodic surfaces: comparison of implicit and explicit solvation models, Phys. Chem. Chem. Phys. 18 (2016) 31850–31861. https://doi.org/10.1039/c6cp04094b.
[76] J. Zhang, H. Zhang, T. Wu, Q. Wang, D. Van Der Spoel, Comparison of Implicit and Explicit Solvent Models for the Calculation of Solvation Free Energy in Organic Solvents, J. Chem. Theory Comput. 13 (2017) 1034–1043. https://doi.org/10.1021/acs.jctc.7b00169.
[77] S. Karimzadeh, B. Safaei, T.C. Jen, Investigate the importance of mechanical properties of SWCNT on doxorubicin anti-cancer drug adsorption for medical application: A molecular dynamic study, J. Mol. Graph. Model. 101 (2020) 107745. https://doi.org/10.1016/j.jmgm.2020.107745.
[78] K. Kita, C. Dittrich, Drug delivery vehicles with improved encapsulation efficiency: Taking advantage of specific drug-carrier interactions, Expert Opin. Drug Deliv. 8 (2011) 329–342. https://doi.org/10.1517/17425247.2011.553216.
[79] L.N.M. Ribeiro, A.C.S. Alcântara, G.H. Rodrigues Da Silva, M. Franz-Montan, S.V.G. Nista, S.R. Castro, V.M. Couto, V.A. Guilherme, E. De Paula, Advances in Hybrid Polymer-Based Materials for Sustained Drug Release, Int. J. Polym. Sci. 2017 (2017). https://doi.org/10.1155/2017/1231464.
[80] I. Rozas, I. Alkorta, J. Elguero, Behavior of ylides containing N, O, and C atoms as hydrogen bond acceptors, J. Am. Chem. Soc. 122 (2000) 11154–11161. https://doi.org/10.1021/ja0017864.

[81] J. Zhang, J. Liu, DFT studies on structural properties and electron density topologies of the iron selenides FemSen ($1 \leq m, n \leq 4$), Russ. J. Phys. Chem. A. 90 (2016) 2564–2570. https://doi.org/10.1134/S0036024416130094.
[82] C. Tantardini, A.A.L. Michalchuk, A. Samtsevich, C. Rota, A.G. Kvashnin, The Volumetric Source Function: Looking Inside van der Waals Interactions, Sci. Rep. 10 (2020) 1–10. https://doi.org/10.1038/s41598-020-64261-4.
[83] J. Netzel, S. Van Smaalen, Topological properties of hydrogen bonds and covalent bonds from charge densities obtained by the maximum entropy method (MEM), Acta Crystallogr. Sect. B Struct. Sci. 65 (2009) 624–638. https://doi.org/10.1107/S0108768109026767.
[84] D. Chudoba, K. Łudzik, M. Jażdżewska, S. Wołoszczuk, Kinetic and Equilibrium Studies of Doxorubicin Adsorption onto Carbon Nanotubes, Int. J. Mol. Sci. 21 (2020) 8230. https://doi.org/10.3390/ijms21218230.
[85] D. Matyszewska, E. Napora, K. Żelechowska, J.F. Biernat, R. Bilewicz, Synthesis, characterization, and interactions of single-walled carbon nanotubes modified with doxorubicin with Langmuir–Blodgett biomimetic membranes, J. Nanoparticle Res. 20 (2018) 143. https://doi.org/10.1007/s11051-018-4239-x.
[86] Glendening, E. D., Reed, A. E., Carpenter, J. E., & Weinhold, F. (1992). NBO, Version 3.1. Pittsburgh: Gaussian, Inc., (n.d.).
[87] Glendening, E.D., Reed, A.E., Carpenter, J.E. and Weinhold F. (2003) NBO Version 3.1. Gaussian Inc., Pittsburgh., (n.d.).
[88] M. Yoosefian, E. Rahmanifar, N. Etminan, Nanocarrier for levodopa Parkinson therapeutic drug; comprehensive benserazide analysis, Artif. Cells, Nanomedicine, Biotechnol. 46 (2018) 434–446. https://doi.org/10.1080/21691401.2018.1430583.
[89] J.S. Murray, P. Politzer, The electrostatic potential: An overview, Wiley Interdiscip. Rev. Comput. Mol. Sci. 1 (2011) 153–163. https://doi.org/10.1002/wcms.19.
[90] J. Murray, K. Sen, Molecular electrostatic potentials: concepts and applications, Elsevier Science B.V., Amsterdam, 1996.

Highlights

- The functionalization of SWCNT enhances DOX adsorption strength and stability.
- The direction of spontaneous electron flow was from DOX molecule to CNT.
- HB interactions play an important role in the stability of DOX/*f*-CNT complexes.
- Negative ΔG and enthalpy values indicated that adsorption process was exothermic.
- Adsorption energy between CNTs and DOX is more in gas phase.